# New Closed-Form Solutions for Optimal Impulsive Control of Spacecraft Relative Motion

Michelle Chernick* and Simone D'Amico†

*Aeronautics and Astronautics, Stanford University, Stanford, California, 94305, USA*

**This paper addresses the fuel-optimal guidance and control of the relative motion for formation-flying and rendezvous using impulsive maneuvers. To meet the requirements of future multi-satellite missions, closed-form solutions of the inverse relative dynamics are sought in arbitrary orbits. Time constraints dictated by mission operations and relevant perturbations acting on the formation are taken into account by splitting the optimal reconfiguration in a guidance (long-term) and control (short-term) layer. Both problems are cast in relative orbit element space which allows the simple inclusion of secular and long-periodic perturbations through a state transition matrix and the translation of the fuel-optimal optimization into a minimum-length path-planning problem. Due to the proper choice of state variables, both guidance and control problems can be solved (semi-)analytically leading to optimal, predictable maneuvering schemes for simple on-board implementation. Besides generalizing previous work, this paper finds four new in-plane and out-of-plane (semi-)analytical solutions to the optimal control problem in the cases of unperturbed eccentric and perturbed near-circular orbits. A general delta-v lower bound is formulated which provides insight into the optimality of the control solutions, and a strong analogy between elliptic Hohmann transfers and formation-flying control is established. Finally, the functionality, performance, and benefits of the new impulsive maneuvering schemes are rigorously assessed through numerical integration of the equations of motion and a systematic comparison with primer vector optimal control.**

## I. Introduction

Control of the relative motion between multiple spacecraft is an important field of study, as future space architectures relying on satellite formation-flying, rendezvous, fractionation, and swarming must adhere to increasingly challenging functional and performance requirements in their Guidance, Navigation, and Control (GNC) tasks.[1] In particular, solutions for formation control and their implementation must comply with reduced on-board resources, such as processing power and propellant, and with tight operational aspects, such as safety, predictability, and time constraints. Based on the experience gained from previous GNC formation-flying demonstrations, such as SAFE,[2] TAFF,[3,4] and ARGON,[5] and from on-going formation-flying mission development efforts, such as AVANTI[6] and mDOT,[7,8] the overall objective of this work is to seek fuel-optimal closed-form solutions of the inverse relative dynamics in perturbed orbits of arbitrary eccentricity. Inspired by previous research in near-circular orbits,[9–11] the fixed-time fixed-end-conditions relative motion reconfiguration is set up through two distinct but interdependent optimization problems. The guidance layer seeks intermediate configurations in the state variables to transfer the formation from the initial to the desired final conditions over an arbitrarily long time interval including time constraints prescribed by the user, whereas the control layer seeks the impulsive maneuvers' size and location to accomplish the said variations in state-space over a short time interval as prescribed by the guidance layer. In order to simplify the search of (semi-)analytical solutions, both optimization problems are conveniently cast in slowly time-varying relative orbit elements (ROE),[9,14] which brings two key benefits. First of all, secular and long-periodic perturbations, such as from Earth's oblateness and differential drag, can be captured by a

*Ph.D. Candidate, Space Rendezvous Laboratory, Aeronautics and Astronautics, Stanford University, 496 Lomita Mall, Stanford, CA 94305.

†Assistant Professor, Space Rendezvous Laboratory, Aeronautics and Astronautics, Stanford University, 496 Lomita Mall, Stanford, CA 94305.

State Transition Matrix (STM) in mean ROE.[12,13] Second, as shown by the Gauss Variational Equations (GVE),[15] the minimum delta-v problem can be translated into a minimum-length path-planning problem in ROE space. This fundamental aspect of the adopted strategy is further demonstrated in this paper through the derivation a new delta-v lower bound for orbits of arbitrary eccentricity, which extends and generalizes previous work in this area done in near-circular orbits.[10,16]

Several formation control algorithms have been described in the literature. The proposed solutions differ in their range of applicability (elliptical or near-circular orbits, separation), their accuracy (inclusion of perturbations) and their mathematical approach (semi-analytical or numerical). Among the numerous numerical methods, Tillerson et al.[17,18] proposed a fuel-optimal strategy based on convex optimization techniques. However, it only partially takes into account perturbations. Roscoe et al.[19] designed an optimal algorithm for elliptical perturbed orbits based on Pontryagin's optimal control and Lawden's primer vector theory[20,21] using the Gim-Alfriend STM.[22] This algorithm employs a discretization of the continuous-time optimal control problem which involves an iterative process that depends on a good initial guess and yields large computational loads. Schaub et al.[23] solves numerically an optimization problem based on the inversion of the GVE without including perturbations. Rogers et al.[24] also uses linear optimal control and a sliding mode tracker to optimize maneuver planning in eccentric orbits. As with most numerical methods, these approaches are computationally expensive and do not provide insight into the optimal size and location of the maneuvers, therefore they do not necessarily represent the best solution for a satellite on-board implementation. Unfortunately, despite its tractability, fewer attempts have been made to solve the optimization problem in closed-form. An analytical solution for the optimal reconfiguration problem was proposed by Vaddi et al[25] in eccentric orbits. It accomplishes the in-plane correction through a couple of impulses in the radial direction of the local orbital frame. A closed-form solution for formation reconfiguration in elliptical orbits has also been derived by Schaub[15] without consideration of optimality and ignoring perturbations. Ichimura and Ichikawa[16] made use of a parameterization defined from the analytical solution of the Hill's equations[26] to develop an analytical, open-time, minimum-fuel reconfiguration strategy based on triplets of maneuvers. Jifuku et al.[27] extended this approach by considering that impulsive maneuvers take place over a finite, limited, and fixed pulses time, but only for circular orbits. Khalil et al.[28] employed integrated GVE as a precise analytical tool to propagate the effects of thrust maneuvers on the ROE. The resulting control schemes are effective and simple enough for on-board implementation, but are limited to only circular chief orbits.

This paper overcomes the observed limitations and builds on the work of D'Amico et al.[9,29] and Gaias et al.[10,11] to offer five main contributions to the state-of-the-art. First of all, the fuel-optimal formation guidance and control problem is formalized so to generalize previous ad-hoc specific approaches. Second, a new general delta-v lower bound is found in orbits of arbitrary eccentricity. This is used to instruct the search of potential closed-form solutions. Third, new semi-analytical fuel-optimal maneuvering schemes are found in perturbed near-circular and unperturbed eccentric orbits, for both in-plane and out-of-plane relative motion control. Fourth, a strong analogy between absolute orbit control (i.e., elliptic Hohmann transfers) and relative orbit control (i.e., formation-flying control) is established. This is used to further assess the optimality of the presented approach. Finally, functionality, performance, and advantages of the new solutions are systematically assessed using numerical integration of the equations of motion and a comparison with primer vector optimal control.[19,30]

After this introduction, Section II presents a review of relative astrodynamics, including the adopted state representation, the governing differential equations and their linearization in the presence of natural perturbations and maneuvers. The state transition and control input matrices used throughout this paper are provided in Section II.A and II.B. Section III formalizes the optimal formation guidance and control problem addressed in this work, including the adopted convex merit functional and the constraints imposed by the relative dynamics. Section IV derives a general delta-v lower bound for eccentric orbits that is later used to instruct the search of optimal solutions of the inverse dynamics and to evaluate their optimality. Section V and VI derive the four new optimal (quasi-)analytical impulsive maneuvering schemes for perturbed near-circular and unperturbed eccentric orbits. Section VII establishes a close analogy between elliptic Hohmann transfers and formation-flying control. Finally, systematic validation of the functionality and performance of the new control solutions is conducted in Section VIII.

## II. Review of Relative Astrodynamics

This research addresses the most general spacecraft formation, which consists of two or more objects flying in close proximity, either cooperatively or non-cooperatively, in elliptic orbits. "Close proximity," as used in this paper, means that the relative motion between the objects can be linearized about the reference orbit, which can be either the physical orbit of one of the objects or a virtual orbit. "Formation," without loss of generality, is assumed to consist of two satellites, namely the chief and the deputy. The "chief" defines the reference orbit and is uncontrolled (or passive), whereas the "deputy" is controlled by a three-dimensional thrust input (or active). The formalism adopted in this work allows a seamless exchange of roles between chief and deputy, or the treatment of an arbitrary number of deputies.

The dynamics of the relative motion can be defined in terms of relative position and velocity (using curvilinear or rectilinear coordinates) in the well-known Hill coordinate frame. Its origin is found at the chief's center of mass (also called radial/along-track/cross-track, RTN, or local-vertical-local-horizontal, LVLH, frame), in terms of combinations (linear or nonlinear) of orbital elements of the chief and deputy, or through alternative representations based on integration constants, canonical epicyclic elements, or quaternion-based, to name the most common. A comprehensive survey of state representations for relative dynamics is provided by Sullivan et al.[31] Besides the geometric interpretation of these variables, the most important difference is given by the differential equations of relative motion resulting from the use of different state representations.[32]

Using non-dimensional Hill's (or RTN) coordinates, $\delta\boldsymbol{x} = (\delta\boldsymbol{r}, \delta\boldsymbol{v})^T$, with relative position $\delta\boldsymbol{r} = (x, y, z)^T$, relative velocity $\delta\boldsymbol{v} = (x', y', z')^T$, and the chief's true anomaly $f_c$ as independent variable, the nonlinear equations of relative motion have the following form[32]

$$\begin{aligned} x'' - 2y' &= \frac{\partial W}{\partial x} + d_x \\ y'' + 2x' &= \frac{\partial W}{\partial y} + d_y \\ z'' &= \frac{\partial W}{\partial z} + d_z \end{aligned} \tag{1}$$

where the pseudo-potential $W = W(\delta\boldsymbol{r}, f_c, e_c)$ is a scalar function of the relative position, true anomaly, and eccentricity of the chief, whereas $\boldsymbol{d} = \boldsymbol{d}_d - \boldsymbol{d}_c = (d_x, d_y, d_z)^T$ represent the normalized differential disturbance and control force expressed in the chief's RTN frame. Using combinations of non-dimensional orbit elements, also called Relative Orbit Elements (ROE), $\delta\boldsymbol{\alpha} = \delta\boldsymbol{\alpha}(\boldsymbol{\alpha}_c, \boldsymbol{\alpha}_d)$, the equations of relative motion can be derived through the Gauss Variational Equations (GVE) expressed in matrix form and applied to each individual satellite as[15]

$$\delta\boldsymbol{\alpha}' = \frac{\partial\delta\boldsymbol{\alpha}}{\partial\boldsymbol{\alpha}_c}\boldsymbol{\alpha}_c' + \frac{\partial\delta\boldsymbol{\alpha}}{\partial\boldsymbol{\alpha}_d}\boldsymbol{\alpha}_d' = \frac{\partial\delta\boldsymbol{\alpha}}{\partial\boldsymbol{\alpha}_c}\boldsymbol{G}(\boldsymbol{\alpha}_c)\boldsymbol{d}_c + \frac{\partial\delta\boldsymbol{\alpha}}{\partial\boldsymbol{\alpha}_d}\boldsymbol{G}(\boldsymbol{\alpha}_d)\boldsymbol{R}_{cd}(\boldsymbol{\alpha}_c, \boldsymbol{\alpha}_d)\boldsymbol{d}_d \tag{2}$$

where the subscripts $c$ and $d$ indicate quantities referring to the chief and deputy spacecraft respectively, the GVE matrix $\boldsymbol{G}$ has dimension (6x3), and the matrix $\boldsymbol{R}_{cd}$ of dimension (3x3) is introduced to rotate vectors from the chief's to the deputy's RTN frame. All matrices are functions of the osculating orbit elements in argument. The most appropriate definition of relative orbit elements $\delta\boldsymbol{\alpha}$ to be used in Eq. 2 depends on the orbit scenario under consideration. It is noted that Eqs. 1 and 2 are perfectly equivalent and hold for elliptic orbits of arbitrary eccentricity. The homogeneous unperturbed solution of Eq. 2 (i.e., when $\boldsymbol{d}_d = \boldsymbol{d}_c = \boldsymbol{0}$) is the trivial solution of the Keplerian two-body problem, $\delta\boldsymbol{\alpha} = const$, whereas no unperturbed solution of Eq. 1 is available in strictly Hill's coordinates.

In the presence of perturbations, as intuition suggests, a state based on ROE is slowly varying with time (or true anomaly) with respect to the orbit period, whereas Hill's coordinates are rapidly varying. In particular, the ROE are affected by secular, long-period, and short-period effects that can be decoupled in a way similar to what was done for the absolute orbit motion in semianalytical and general perturbation approaches used in well diffused satellite orbital motion propagators such as the Draper Semianalytical Satellite Theory or the Simplified General Perturbations theory.[33] The benefit of this approach is also given by the fact that short-period variations of the absolute orbit elements, $(\boldsymbol{\alpha}_c, \boldsymbol{\alpha}_d)$ are a function of the location of the spacecraft along the reference trajectory and can often be neglected for orbit design and control when differenced to form ROE in $\delta\boldsymbol{\alpha} = \delta\boldsymbol{\alpha}(\boldsymbol{\alpha}_c, \boldsymbol{\alpha}_d)$.[34]

The need to design GNC systems for formation-flying and rendezvous has motivated many authors to linearize Eqs. 1 and 2 for small nondimensional state parameters. In particular, the linearization of Eq. 1 leads to the Tschauner-Hempel equations[35] for arbitrary eccentricity and to the Hill-Clohessy-Wiltshire equations for near-circular orbits.[26] Unfortunately, the closed-form solutions of these equations are affected

by major limitations, such as the small range of applicability and the neglect of perturbation forces. On the contrary, averaging theory[32] can be used to first incorporate non-Keplerian perturbations (from conservative and non-conservative forces, including maneuvers) and then expand Eq. 2 into a Taylor expansion around the reference orbit elements.[13] Neglecting second order terms in the ROE which are multiplied by non-null partial derivatives leads to a linear dynamics system which is valid in the presence of perturbations and for larger separations between the spacecraft. The resulting closed-form solution for the evolution of the mean ROE in the interval $[t_0, t_f]$ is of the form[11,19]

$$\delta\boldsymbol{\alpha}(t_f) = \boldsymbol{\Phi}_{f,0}\delta\boldsymbol{\alpha}(t_0) + \boldsymbol{\Phi}_{f,1}\boldsymbol{\Gamma}_1\delta\boldsymbol{v}_1 + ... + \boldsymbol{\Phi}_{f,p}\boldsymbol{\Gamma}_p\delta\boldsymbol{v}_p \tag{3}$$

where $\boldsymbol{\Phi}_{f,i} = \boldsymbol{\Phi}(t_f, t_i)$ with $i = 0, 1, ..., p$, is the State Transition Matrix (STM), $\boldsymbol{\Gamma}_k$ with $k = 1, ..., p$ is the control input matrix, and the vectors $\delta\boldsymbol{v} = (\delta v_R, \delta v_T, \delta v_N)^T$ represent $p$ impulsive maneuvers expressed in the deputy's RTN frame. It is noted that here $t$ represents the independent variable of choice and not time necessarily. The adoption of impulsive delta-v's implies maneuvers of short duration as compared with the orbit period which cause an instantaneous variation of the spacecraft velocity with no change of position. In this paper, the state is defined as the following combination of mean absolute orbit elements[34]

$$\delta\boldsymbol{\alpha} = \begin{bmatrix} \delta a \\ \delta\lambda \\ \delta e_x \\ \delta e_y \\ \delta i_x \\ \delta i_y \end{bmatrix} = \begin{bmatrix} \delta a \\ \delta\lambda \\ \delta e\cos\phi \\ \delta e\sin\phi \\ \delta i\cos\theta \\ \delta i\sin\theta \end{bmatrix} = \begin{bmatrix} \frac{a_d - a_c}{a_c} \\ u_d - u_c + (\Omega_d - \Omega_c)\cos(i_c) \\ e_d\cos(\omega_d) - e_c\cos(\omega_c) \\ e_d\sin(\omega_d) - e_c\sin(\omega_c) \\ i_d - i_c \\ (\Omega_d - \Omega_c)\sin(i_c) \end{bmatrix} \tag{4}$$

which is composed of the relative eccentricity vector, $\delta\boldsymbol{e} = \boldsymbol{e}_d - \boldsymbol{e}_c$, the relative inclination vector, $\delta\boldsymbol{i}$, the relative semi-major axis, $\delta a$, the relative mean longitude $\delta\lambda$, and the mean argument of latitude, $u = M + \omega$. The state of choice is valid for circular orbits ($e_c = 0$), but is still singular for equatorial orbits ($i_c = 0$). For near-circular reference orbits, the ROE describe the section of an elliptic cylinder in Hill's coordinates.[32] In particular, $\delta\boldsymbol{e}$ and $\delta\boldsymbol{i}$ drive the amplitude of periodic in-plane (RT) and out-of-plane (N) oscillations respectively, whereas $\delta\lambda$ and $\delta a$ provide offsets in along-track (T) and radial (R) directions respectively.[34] For elliptic reference orbits, an additional mode is superimposed at twice the frequency with amplitude proportional to the eccentricity of the reference orbit. This state is at the basis of the GNC and orbit design of a number of formation-flying missions such as GRACE,[36] PRISMA,[2] and TanDEM-X.[3]

STMs which include Earth's geopotential J2-J3, drag, solar radiation pressure, and third-body effects on the mean ROE defined by Eq. 4 have been derived recently[13,37] for orbits of arbitrary eccentricity. In order to find closed-form optimal delta-v solutions through the inversion of Eq. 3, the complexity of these STMs is reduced by considering only the dominant effects on the relative dynamics. In the case of J2-only perturbations, the STM over the time interval $[t_0, t_f]$ is given by[13]

$$\boldsymbol{\Phi}_{f,0} = \begin{bmatrix} 1 & 0 & 0 & 0 & 0 & 0 \\ -\frac{7}{2}\kappa EP\tau - \frac{3}{2}\eta\tau & 1 & \kappa e_{x0}FGP\tau & \kappa e_{y0}FGP\tau & -\kappa FS\tau & 0 \\ \frac{7}{2}\kappa e_{yf}Q\tau & 0 & \cos(\dot{\omega}\tau) - 4\kappa e_{x0}e_{yf}GQ\tau & -\sin(\dot{\omega}\tau) - 4\kappa e_{y0}e_{yf}GQ\tau & 5\kappa e_{yf}S\tau & 0 \\ -\frac{7}{2}\kappa e_{xf}Q\tau & 0 & \sin(\dot{\omega}\tau) + 4\kappa e_{x0}e_{xf}GQ\tau & \cos(\dot{\omega}\tau) + 4\kappa e_{y0}e_{xf}GQ\tau & -5\kappa e_{xf}S\tau & 0 \\ 0 & 0 & 0 & 0 & 1 & 0 \\ \frac{7}{2}\kappa S\tau & 0 & -4\kappa e_{x0}GS\tau & -4\kappa e_{y0}GS\tau & 2\kappa T\tau & 1 \end{bmatrix} \tag{5}$$

where

$$\begin{array}{cccc} \gamma = \frac{3}{4}J_2R_e^2\sqrt{\mu}, & \eta = \sqrt{1 - ||\boldsymbol{e}||^2}, & \kappa = \frac{\gamma}{a^{\frac{7}{2}}\eta^4} & G = \frac{1}{\eta^2} \\ E = 1 + \eta, & F = 4 + 3\eta, & T = \sin^2 i & \tau = t_f - t_0 \\ P = 3\cos^2 i - 1, & Q = 5\cos^2 i - 1, & S = \sin 2i & \dot{\omega} = \kappa Q \end{array} \tag{6}$$

the subscripts 0 and $f$ denote initial and final values of the chief's orbit elements respectively, the subscript $c$ is dropped after linearization since absolute orbit elements of chief and deputy can be exchanged

without loss of accuracy, $\mu$ is the Earth's gravitational parameter, $R_e$ is the Earth's equatorial radius, and $n$ is the mean motion of the chief spacecraft. Note that the usage of the mean anomaly, $M$, and the relative mean longitude, $\delta\lambda$, makes the STM given by Eq. 5 simpler than the well-known STM developed by Gim and Alfriend.[22] The dominant secular and long-period effects caused by J2 on the mean ROE as given by Eq. 5 are illustrated in Fig. 1. The relative eccentricity vector results from a superposition of a harmonic oscillator and a linear drift perpendicular to the absolute eccentricity vector. The relative inclination vector draws a vertical line with a speed proportional to its x-component. The relative semi-major axis and mean longitude follow a quadratic curve with apex at $\delta a = 0$. The knowledge of these trends is extremely useful to define control windows in ROE-space for fuel-optimal maneuver planning as previously done in near-circular orbits.[9,29]

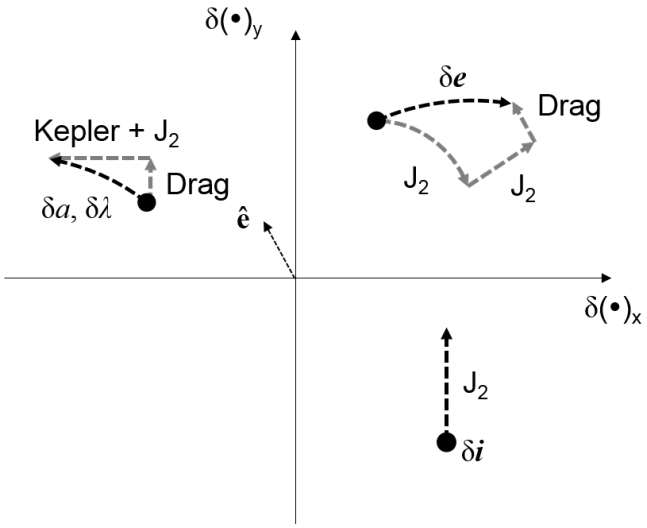


Figure 1: Notional illustration of differential J2 and drag secular and long-period effects on ROE for orbits of arbitrary eccentricity. The unit eccentricity vector of the chief orbit is indicated by $\hat{\boldsymbol{e}}$. Individual contributions (gray arrows) sum up to the total trend (black arrows) in ROE space.

The effect of impulsive maneuvers is again captured by the GVE. In particular, the control input matrix, $\boldsymbol{\Gamma}_k$, introduced in Eq. 3 can be derived by integrating Eq. 2 over the course of the maneuver neglecting all other perturbations. Enforcing our linearization assumption in ROE allows for the superposition of effects and is equivalent to assuming small delta-v's. As a consequence, the absolute orbit elements of the maneuvering spacecraft remains effectively constant during the integration, and the effects on mean and osculating orbit elements can be considered identical, resulting in

$$\Delta\delta\boldsymbol{\alpha}_k = \boldsymbol{\Gamma}_k\delta\boldsymbol{v}_k = \frac{\partial\delta\boldsymbol{\alpha}}{\partial\boldsymbol{\alpha}}\boldsymbol{G}(\boldsymbol{\alpha})\delta\boldsymbol{v}_k \tag{7}$$

It is noted that the operator $\Delta$ represents the arithmetic difference between ROE after and before the impulsive maneuver, and that the variation of ROE is equivalent to a total variation of the mean orbit elements of the maneuvering spacecraft. The explicit expression of $\boldsymbol{\Gamma}_k$ is provided in the next sections as tailored to the cases of near-circular and eccentric orbits.

### A. Perturbed Near-Circular Orbits

For zero eccentricity of the chief (or reference) orbit (i.e., $e = 0$), the STM given by Eq. 5 can be simplified to[12,13]

$$\boldsymbol{\Phi}_{f,0} = \begin{bmatrix} 1 & 0 & 0 & 0 & 0 & 0 \\ -\frac{7\kappa P+3n}{2}\tau & 1 & 0 & 0 & -4\kappa S\tau & 0 \\ 0 & 0 & \cos(\dot{\omega}\tau) & -\sin(\dot{\omega}\tau) & 0 & 0 \\ 0 & 0 & \sin(\dot{\omega}\tau) & \cos(\dot{\omega}\tau) & 0 & 0 \\ 0 & 0 & 0 & 0 & 1 & 0 \\ \frac{7}{2}\kappa S\tau & 0 & 0 & 0 & 2\kappa T\tau & 1 \end{bmatrix} \tag{8}$$

where $\dot{\omega}$ is the precession rate of the reference absolute eccentricity vector which matches the angular rate of the relative eccentricity vector. For impulsive maneuver planning, it is convenient to use the mean argument of latitude $u = M + \omega$ instead of time as independent variable. The resulting STM is obtained from Eq. 8 by substituting

$$\tau = \frac{\Delta u}{n + \kappa(\eta P + Q)} \tag{9}$$

where the time interval has been replaced by the mean argument of latitude interval $\Delta u = u_f - u_0$, including $J_2$ secular effects on the reference orbit. The effects of an impulsive maneuver executed at the mean argument of latitude $u_k$ is given by Eq. 7 adapted to near-circular orbits as[14]

$$\Delta\delta\boldsymbol{\alpha}_k = \boldsymbol{\Gamma}_k\delta\boldsymbol{v}_k = \frac{1}{na}\begin{bmatrix} 0 & 2 & 0 \\ -2 & 0 & 0 \\ \sin(u_k) & 2\cos(u_k) & 0 \\ -\cos(u_k) & 2\sin(u_k) & 0 \\ 0 & 0 & \cos(u_k) \\ 0 & 0 & \sin(u_k) \end{bmatrix}\begin{bmatrix} \delta v_R \\ \delta v_T \\ \delta v_N \end{bmatrix} \tag{10}$$

It is noteworthy that the effects of in-plane and out-of-plane maneuvers are fully decoupled thanks to our choice of ROE within the adopted linearization assumptions. Due to their simplicity, Eqs. 8-10 allow for new closed-form solutions of the orbit control problem based on the inversion of Eq. 3 as shown in the sequel.

### B. Unperturbed Eccentric Orbits

For eccentric orbits it is convenient to replace the relative mean longitude, $\delta\lambda$, with a modified state parameter, $\delta\lambda_e$, the modified relative mean longitude, which is defined as

$$\delta\lambda_e = M_d - M_c + \eta(\omega_d - \omega_c + (\Omega_d - \Omega_c)\cos(i_c)) \tag{11}$$

Such a change of state parameter eliminates the direct effect of a tangential maneuver on the modified relative mean longitude, and therefore simplifies the dynamics of the reconfiguration.[30] For unperturbed eccentric orbits (i.e., $J_2 = 0$), the STM given by Eq. 5 can be simplified to[15]

$$\boldsymbol{\Phi}_{f,0} = \begin{bmatrix} 1 & 0 & 0 & 0 & 0 & 0 \\ -\frac{3}{2}\Delta M & 1 & 0 & 0 & 0 & 0 \\ 0 & 0 & 1 & 0 & 0 & 0 \\ 0 & 0 & 0 & 1 & 0 & 0 \\ 0 & 0 & 0 & 0 & 1 & 0 \\ 0 & 0 & 0 & 0 & 0 & 1 \end{bmatrix} \tag{12}$$

where the propagation interval is now described by the change of mean anomaly $\Delta M = M_f - M_0$. The effects of an impulsive maneuver executed at the true argument of latitude $\theta_k = \nu_k + \omega_k$ is given by Eq. 7 adapted to our choice of ROE[30]

$$\Delta\delta\boldsymbol{\alpha}_k = \boldsymbol{\Gamma}_k\delta\boldsymbol{v}_k = \frac{1}{na}\begin{bmatrix} \frac{2}{\eta}e\sin\nu_k & \frac{2}{\eta}(1+e\cos\nu_k) & 0 \\ -\frac{2\eta^2}{1+e\cos\nu_k} & 0 & 0 \\ \eta\sin\theta_k & \eta\frac{(2+e\cos\nu_k)\cos\theta_k+e_x}{1+e\cos\nu_k} & \frac{\eta e_y}{\tan(i)}\frac{\sin\theta_k}{1+e\cos\nu_k} \\ -\eta\cos\theta_k & \eta\frac{(2+e\cos\nu_k)\sin\theta_k+e_y}{1+e\cos\nu_k} & -\frac{\eta e_x}{\tan(i)}\frac{\sin\theta_k}{1+e\cos\nu_k} \\ 0 & 0 & \eta\frac{\cos\theta_k}{1+e\cos\nu_k} \\ 0 & 0 & \eta\frac{\sin\theta_k}{1+e\cos\nu_k} \end{bmatrix}\begin{bmatrix}\delta v_R \\ \delta v_T \\ \delta v_N\end{bmatrix} \tag{13}$$

As expected, the control input matrix for eccentric orbits reduces to Eq. 10 when $e = 0$. Although the sparsity of the two matrices is similar, in contrast to the near-circular case, now variations of the relative semi-major axis and relative eccentricity vector are also caused by maneuvers in radial and cross-track direction respectively. It is noted that the effect of cross-track maneuvers on the relative eccentricity vector can be removed by redefining the relative eccentricity vector as

$$\begin{bmatrix}\delta e_{e_x} \\ \delta e_{e_y}\end{bmatrix} = \begin{bmatrix} e_d - e_c \\ \omega_d - \omega_c + (\Omega_d - \Omega_c)\cos i_c\end{bmatrix} \tag{14}$$

The modified relative mean longitude and relative inclination vector are only affected by radial and cross-track maneuvers, respectively, similar to the near-circular case. Due to their simplicity, Eqs. 12-13 allow for new closed-form solutions of the orbit control problem based on the inversion of Eq. 3 as shown in the sequel.

## III. Optimal Formation Guidance and Control

A spacecraft formation reconfiguration is defined as the transfer from a given initial state, $\delta\boldsymbol{\alpha}_0$, to a known target final state, $\delta\boldsymbol{\alpha}_f$, over a finite interval of the independent variable of choice, being it time, mean or true argument of latitude. The overall objective of this work is to find closed-form solutions for the sequence of impulsive maneuvers which accomplish the reconfiguration above, employing the minimum delta-v budget. Similar to Gaias et al.,[11] Eq. 3 is split in two parts without loss of generality

$$\begin{aligned}\Delta\delta\bar{\boldsymbol{\alpha}} &= \delta\boldsymbol{\alpha}(t_f) - \boldsymbol{\Phi}_{f,0}\delta\boldsymbol{\alpha}(t_0) = \boldsymbol{\Phi}_{f,1}\Delta\delta\bar{\boldsymbol{\alpha}}_1 + \boldsymbol{\Phi}_{f,2}\Delta\delta\bar{\boldsymbol{\alpha}}_2 + ... + \boldsymbol{\Phi}_{f,m}\Delta\delta\bar{\boldsymbol{\alpha}}_m \\ \Delta\delta\bar{\boldsymbol{\alpha}}_j &= \delta\boldsymbol{\alpha}(t_{f_j}) - \boldsymbol{\Phi}_{f_j,0_j}\delta\boldsymbol{\alpha}(t_{0_j}) = \bar{\boldsymbol{\Phi}}_{j,1}\boldsymbol{\Gamma}_1\delta\boldsymbol{v}_1 + \bar{\boldsymbol{\Phi}}_{j,2}\boldsymbol{\Gamma}_2\delta\boldsymbol{v}_2 + ... + \bar{\boldsymbol{\Phi}}_{j,N}\boldsymbol{\Gamma}_N\delta\boldsymbol{v}_N\end{aligned} \tag{15}$$

where the first equation describes $m$ unknown variations of the ROE to be accomplished during the complete reconfiguration, and the second equation groups the overall effect of a series of $N$ unknown impulsive maneuvers on the individual variations of ROE, $\Delta\delta\bar{\boldsymbol{\alpha}}_j$, with $j = 1, ..., m$. The key idea is to split an arbitrary large reconfiguration into a guidance (or global) problem governed by the first of Eq. 15 and into a control (or local) problem governed by the second of Eq. 15. The guidance problem seeks $m$ intermediate states or formation configurations to be acquired over a long duration where non-Keplerian perturbations are important. This requires the adoption of an accurate STM, $\boldsymbol{\Phi}$, in the first of Eq. 15. The control problem seeks the $N$ maneuvers' size and location to realize the said ROE individual variations (or the guidance profile) in a short time interval where non-Keplerian perturbations can be neglected. This allows the usage of a simplified STM, $\bar{\boldsymbol{\Phi}}$, in the second of Eq. 15. As a consequence, the fuel-optimal guidance and control problems are now tractable in closed-form and can be tackled separately. In addition, the typical time constraints dictated by space mission operations can be seamlessly incorporated into the first of Eq. 15 by fixing the time intervals $[t_{0_j}, t_{f_j}]$ over which the desired variations $\Delta\delta\bar{\boldsymbol{\alpha}}_j$ have to occur.

In particular, the guidance problem seeks to minimize the following convex functional

$$J_{guid} = \sum_{j=1}^{m}||\Delta\delta\bar{\boldsymbol{\alpha}}_j||^2 = \sum_{j=1}^{m}||\Delta\delta\boldsymbol{i}_j||^2 + \sum_{j=1}^{m}(\Delta\delta a_j)^2 + \sum_{j=1}^{m}(\Delta\delta\lambda_j)^2 + \sum_{j=1}^{m}||\Delta\delta\boldsymbol{e}_j||^2 \tag{16}$$

subject to the dynamics constraint from the first of Eq. 15, which are re-written in compact form as the following linear system of 6 equations in $6m$ unknowns

$$\Big[\boldsymbol{\Phi}_{f,1}(:,1) \quad .. \quad \boldsymbol{\Phi}_{f,m}(:,1) \quad \boldsymbol{\Phi}_{f,1}(:,2) \quad .. \quad \boldsymbol{\Phi}_{f,m}(:,2) \quad .. \quad \boldsymbol{\Phi}_{f,1}(:,6) \quad .. \quad \boldsymbol{\Phi}_{f,m}(:,6)\Big] \begin{bmatrix} \Delta\delta\bar{\alpha}_{1,1} \\ \Delta\delta\bar{\alpha}_{1,2} \\ .. \\ \Delta\delta\bar{\alpha}_{1,m} \\ .. \\ \Delta\delta\bar{\alpha}_{6,1} \\ \Delta\delta\bar{\alpha}_{6,2} \\ .. \\ \Delta\delta\bar{\alpha}_{6,m} \end{bmatrix} = \Delta\delta\bar{\boldsymbol{\alpha}} \tag{17}$$

The (6x6m) matrix on the left hand side of Eq. 17 is assembled from the columns of the original STM, $\boldsymbol{\Phi}(:, i = 1, ..., 6)$, in Eq. 15. The solution process[11] derives an expression for $\Delta\delta\bar{\boldsymbol{\alpha}}_m$ as a function of the first $m-1$ variations of ROE from the first of Eq. 15. This expression is then substituted in Eq. 16 to provide a cost functional which is only a function of the $m-1$ variations of ROE. The necessary and sufficient conditions for optimality are then given by nulling the partial derivatives of $J_{guid}$ with respect to the unknowns. The optimal solution reduces to solving a linear system in the problem's variables. In other words, the particular choice of state representation allows solving the optimum problem for the dynamical system as a geometrical path planning problem, whose solution is the most convenient succession of reachable points in ROE space (see Fig. 2). The closed-form solution of the guidance problem for perturbed near-circular orbits has been found[11] when the small cross-coupling terms, $\boldsymbol{\Phi}(2,5)$ and $\boldsymbol{\Phi}(1,6)$, between in-plane and out-of-plane ROE of the STM given by Eq. 8 are neglected. More general solutions for near-circular orbits and for the case of perturbed eccentric orbits are not available to date (i.e., using the STM from Eq. 5).

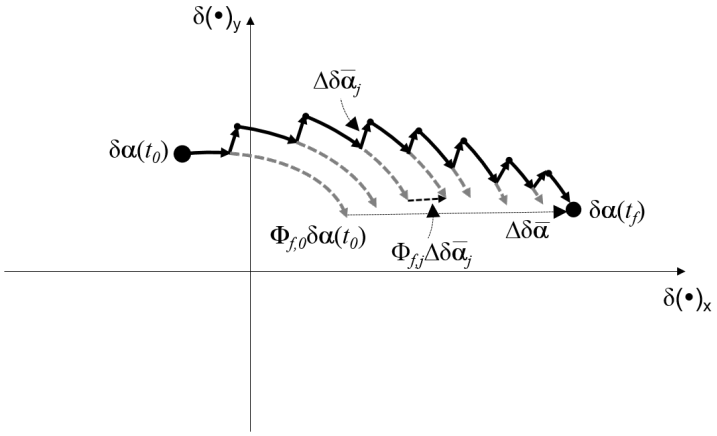


Figure 2: Notional illustration of guidance plan in ROE space including perturbations. The geometric meaning of each 6-D vector appearing in the first of Eq. 15 is illustrated. The trajectory resulting from the optimization (black line) corresponds to the minimal path from initial to final state in the presence of perturbations.

This paper focuses on the control (shorter term) problem which seeks to minimize the following convex functional

$$J_{ctrl} = \Big(\sum_{k=1}^{N} ||\delta\boldsymbol{v}_k||\Big)^2 = \Big(\sum_{k=1}^{N} \sqrt{\delta v_{R_k}^2 + \delta v_{T_k}^2 + \delta v_{N_k}^2}\Big)^2 \tag{18}$$

subject to the dynamics constraint from the second of Eq. 15, which are re-written in compact form as the following linear system of 6 equations in $4N$ unknowns given by $3N$ delta-v components in RTN and $N$ maneuver execution times (or locations)

$$\begin{bmatrix} \bar{\mathbf{\Phi}}_{j,1}\mathbf{\Gamma}_1 & \bar{\mathbf{\Phi}}_{j,2}\mathbf{\Gamma}_2 & .. & \bar{\mathbf{\Phi}}_{j,N}\mathbf{\Gamma}_N \end{bmatrix} \begin{bmatrix} \delta\boldsymbol{v}_1 \\ \delta\boldsymbol{v}_2 \\ .. \\ \delta\boldsymbol{v}_N \end{bmatrix} = \boldsymbol{M}_{[6,3N]}\delta\boldsymbol{v}_{[3N,1]} = \Delta\delta\bar{\boldsymbol{\alpha}}_j \tag{19}$$

It is noteworthy that Eq. 19 represents a re-arrangement of Eq. 17 where jumps in ROE are replaced by maneuver delta-vs. However, the maneuver application times are now unknown, and the STM used for control, $\bar{\mathbf{\Phi}}$, can be simplified due to the short time interval. This is especially true if the guidance problem describes a trajectory arc of tens of orbits (e.g., days in low Earth orbit), whereas the control window is only a few orbits long (e.g., hours in low Earth orbit). The extra-fuel expenditure or sub-optimality introduced by the simplification of the STM in the left hand side of Eq. 19 increases with the length of the control window $[t_{0_j}, t_{f_j}]$ and with the varying effects of perturbations caused by the intermediate maneuvers. Considering Keplerian-only relative motion for $\bar{\mathbf{\Phi}}$ over the control interval (cf. Eq. 8 and 12), Eq. 19 represents two disjoint systems of linear equations, describing the in-plane (4 equations in $3N$ unknowns) and out-of-plane (2 equations in $2N$ unknowns) reconfiguration problems. This is true for both near-circular and eccentric reference orbits if the proper set of ROE is adopted as described in Sec. II. In addition, Eq. 19 fixes the minimum number of maneuvers required to meet an arbitrary set of end conditions, $\Delta\delta\bar{\boldsymbol{\alpha}}_j \neq \mathbf{0}$, for each control problem. In particular, one cross-track maneuver, $N = 1$, is necessary and sufficient for the out-of-plane reconfiguration, whereas two or more in-plane maneuvers, $N \geq 2$, are necessary for the in-plane reconfiguration. In the case that only radial or tangential maneuvers are employed, the in-plane reconfiguration is governed by 4 equations in $2N$ unknowns, and two in-plane maneuvers provide a fully determined system of linear equations without extra degrees of freedom for fuel optimization. As shown by Gaias and D'Amico,[10] maneuvering schemes with $N = 2$ generally requires to be solved numerically with proper initial conditions and cannot achieve the absolute minimum delta-v cost. Although previous flight demonstrations (i.e., SAFE,[2] TAFF,[4] ARGON[5]) exploited the analytical expression of a pair of tangential/radial maneuvers to accomplish in-plane formation control, despite their simplicity, these particular solutions can only establish three desired ROE after execution. As a consequence, multiple pairs of maneuvers and a dedicated guidance plan were necessary to complete the most general reconfiguration. On the contrary, maneuvering schemes with $N = 3$ allow for analytical or semi-analytical solutions that are able to meet the minimum delta-v cost. Such closed-form solutions have been found in the case of purely Keplerian relative motion in near-circular orbits.[10] To improve performance and range of applicability, this paper derives new closed-form solutions for orbit control using triplets of in-plane maneuvers and single out-of-plane maneuvers in the more general cases of perturbed near-circular and unperturbed eccentric orbits driven by the dynamics described in Sec. II.

## IV. Delta-v Lower Bound for Formation Control

In order to instruct the search of closed-form optimal solutions of the control problem described by Eq. 18 and 19, it is convenient to analyze the so-called delta-v lower bound, $\delta v_{LB}$, for in-plane formation control. The delta-v lower bound represents the absolute minimum required delta-v for any given reconfiguration. In other words, the merit functional evaluated at the optimal delta-v solution, $J_{ctrl}(\delta\boldsymbol{v})$, is always larger than or equal to $\delta v_{LB}^2$. The delta-v lower bound also represents a quick way to assess the optimality of proposed delta-v solutions. For eccentric orbits, the instantaneous variation of ROE caused by an impulsive maneuver is given by Eq. 13, whereas the STM from Eq. 12 provides the eventually propagated effect of the maneuver after its execution. The most efficient maneuver direction for a given change in ROE can be found by comparing the normalized effect of a unit size delta-v on the ROE. This is done systematically in Table 1 by inspection of the aforementioned equations. In contrast to near-circular orbits, both radial and tangential impulsive maneuvers affect the relative semi-major axis in eccentric orbits. From Eq. 13, the minimum radial burn for a change in $\delta a$ occurs at true anomaly $\nu = \frac{\pi}{2}$ (i.e., semi-latus rectum), and its normalized effect is given by $\frac{2}{\eta}e$. Proceeding similarly, the minimum tangential burn for a change in $\delta a$ occurs at $\nu = 0$ (i.e., periapsis), where the velocity is maximum and tangent to the orbit. Its normalized effect is given by $\frac{2}{\eta}(1+e)$. Since $\frac{2}{\eta}(1+e) > \frac{2}{\eta}e$, the most efficient tangential burn is always smaller than the most efficient radial burn. The corresponding delta-v lower bound for a change in relative semi-major axis is given by tangential maneuvers as provided in the last column of Table 1.

Table 1: Effect of unitary $\delta v$ in radial and along-track direction on in-plane ROE during control interval identified by a shift of mean anomaly $\Delta M$

| ROE change | Direction of maneuver | Optimal location | Max normalized effect | Delta-v lower bound $[m/s]$ |
|---|---|---|---|---|
| $\Delta\delta a$ | Radial | $\nu = \frac{\pi}{2}, \frac{3}{2}\pi, ...$ | $\frac{2}{\eta}e$ | |
| | Tangential | $\nu = 0$ | $\frac{2}{\eta}(1+e)$ | $\frac{\eta}{2(1+e)}na\lvert\Delta\delta\bar{a}\rvert$ |
| $\Delta\delta\lambda_e$ | Radial | $\nu = \frac{\pi}{2}, \frac{3}{2}\pi, ...$ | $\frac{3}{\eta}e\Delta M + 2\eta^2$ | $\frac{\eta}{3e\Delta M+2\eta^3}na\lvert\Delta\delta\bar{\lambda_e}\rvert$ or |
| | Tangential | $\nu = 0$ | $\frac{3}{\eta}e\Delta M + \frac{3}{\eta}\Delta M$ | $\frac{\eta}{3(1+e)\Delta M}na\lvert\Delta\delta\bar{\lambda_e}\rvert$ |
| $\lvert\lvert\Delta\delta\boldsymbol{e}_e\rvert\rvert$ | Radial | Anywhere | $\eta$ | |
| | Tangential | $\nu = k\pi,$ $k = 0, 1, ...$ | $2\eta$ | $\frac{1}{2\eta}na\lvert\lvert\Delta\delta\bar{\boldsymbol{e}}\rvert\rvert$ |

An aimed variation of $\delta\lambda_e$ can be achieved through a tangential or radial delta-v which introduces the proper drift in modified relative mean longitude for the duration of the reconfiguration. It is noted that radial maneuvers, in addition to the drift, provide a direct shift of $\delta\lambda_e$ given by $2\eta^2$ at best. As a result, tangential maneuvers are more efficient than radial maneuvers in the case that $\frac{3}{\eta}\Delta M > 2\eta^2$, or $\Delta M > 2\eta^3/3$. Since $0 \leq \eta \leq 1$, this condition translates to a reconfiguration span of $\Delta M = [0.0, 38.2]$ degrees, dependent on the reference eccentricity, where radial maneuvers provide the delta-v lower bound for changes of modified relative mean longitude. The limit cases are provided by a control window of zero degrees, where only radial maneuvers can affect the modified relative mean longitude, and 38.2 degrees, for a circular orbit.

Finally the relative eccentricity vector, as defined by Eq. 14, can be changed by radial and tangential maneuvers. From Eq. 13, the normalized effect of a unit radial impulse $||\Delta\delta\boldsymbol{e}||$ is not dependent on the maneuver location and equals $\eta$. The normalized effect of a unitary tangential impulse is given by

$$||\Delta\delta\boldsymbol{e}|| = \eta\frac{\sqrt{(2+e\cos\nu)^2 + e^2 + 2e(2+e\cos\nu)\cos\nu}}{1+e\cos\nu} \tag{20}$$

whose minimum equals $2\eta$ at $\nu = k\pi$, where $k$ is an integer. Thus, a tangential burn always has at least twice the effect on $||\Delta\delta\boldsymbol{e}||$ as compared with a radial burn. The resulting $\delta v_{LB}$ for the relative eccentricity vector is given by tangential maneuvers. From the last column of Table 1, the most general delta-v lower bound for orbits of arbitrary eccentricity is given by

$$\delta v_{LB}/na\eta = \max(\frac{|\Delta\delta\bar{a}|}{2(1+e)}, \frac{|\Delta\delta\bar{\lambda_e}|}{K(e,\Delta M)}, \frac{||\Delta\delta\bar{\boldsymbol{e}}||}{2\eta^2}) \tag{21}$$

where $K(e, \Delta M) = \max(3e\Delta M + 2\eta^3, 3(1+e)\Delta M)$. This newly derived delta-v lower bound reduces to the following simplified form for circular orbits

$$\delta v_{LB}/na = \max(\frac{|\Delta\delta\bar{a}|}{2}, \frac{|\Delta\delta\bar{\lambda_e}|}{\max(2, 3\Delta M)}, \frac{||\Delta\delta\bar{\boldsymbol{e}}||}{2}) \tag{22}$$

where $\eta = 1$ and $e = 0$ have been substituted in Eq. 21. These findings generalize previous approaches to orbits of arbitrary eccentricity, and introduce a slight correction of the delta-v lower bound for near-circular orbits which accounts for the potential superiority of radial maneuvers for relative mean longitude control over short control windows. Fundamentally, Eq. 21 shows that the task of minimizing fuel for formation control is equivalent to minimizing the length of the path taken from initial to final conditions in ROE space. The cost of any reconfiguration is driven by the largest variation among relative semi-major axis, relative mean longitude, and relative eccentricity vector. Since the lower delta-v bound for in-plane control can only be reached through along-track maneuvers in the most general reconfiguration, the following sections seek closed-form solutions neglecting the radial component. Similar to the effects of perturbations, along-track and cross-track maneuvers cause changes of the individual ROE as depicted in Fig. 3.

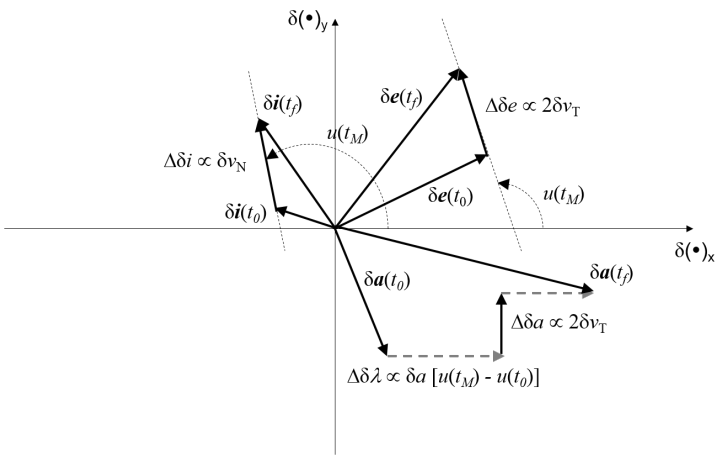


Figure 3: Notional illustration of effects of impulsive along-track and cross-track maneuvers in ROE space for near-circular orbits. Maneuver's location and size drive the orientation and length of the ROE variations.

The orientation (or phase) of the variation of the relative eccentricity and inclination vectors, $\Delta\delta()$, match the mean argument of latitude of the maneuver, $u(t_M)$. Also, the length of the variation-vector is proportional to the size of the maneuver. For eccentric orbits, the trends shown in Fig. 3 are similar but change slightly. In particular, the orientation of the variation-vector is now driven by the true argument of latitude of the maneuver, $\theta(t_M) = \nu(t_M) + \omega(t_M)$. In addition to being proportional to the size of the maneuvers, the length of the variation-vector becomes a function of the maneuver location as well. Radial maneuvers cause effects similar to tangential maneuvers with relative eccentricity vector's variations which are approximately half in length and have orientations given by $\theta(t_M)+\pi/2$. Combining the results depicted in Fig. 2 and Fig. 3 leads to a fully geometrical approach to formation-flying planning and control. It is finally noted that the delta-v lower bound given by Eq. 21 has been derived for the problem described by Eq. 19 adopting a STM, $\bar{\mathbf{\Phi}}$, which takes into account only Keplerian effects. Although perturbations are taken into account by pre-compensation through a proper computation of the desired total variation $\Delta\delta\bar{\boldsymbol{\alpha}}_j$, residual $J_2$ effects caused by the change of ROE by individual maneuvers during the reconfiguration might slightly reduce $\delta v_{LB}$.

## V. Control in Perturbed Near-Circular Orbits

### A. Out-of-plane Reconfiguration

Previous authors have considered Earth's oblateness $J_2$ effects acting on the relative inclination vector through the guidance layer only. As explained in Sec. III, this is done by pre-compensating the total effect of this perturbation over the reconfiguration interval by computing $\Delta\delta\bar{\boldsymbol{i}} = \delta\boldsymbol{i}(t_f) - \mathbf{\Phi}_{f,0}\delta\boldsymbol{i}(t_0)$. A Keplerian-only relative motion model for $\bar{\mathbf{\Phi}}_{j,1}$ is then used for maneuver planning to realize $\Delta\delta\bar{\boldsymbol{i}}$ which does not capture the potential $J_2$ effects caused by the modified state after the single cross-track maneuver. The resulting closed-form control solution is given by[9]

$$\begin{aligned} u_N &= \arctan\tfrac{\Delta\delta\bar{i}_y}{\Delta\delta\bar{i}_x} \\ |\delta v_N| &= na||\Delta\delta\bar{\boldsymbol{i}}|| \end{aligned} \tag{23}$$

Here, an attempt is made to improve performance by using $\mathbf{\Phi}$ from Eq. 8 for the complete out-of-plane reconfiguration. The dynamics equations governing the relative inclination vector are

$$\begin{aligned} \cos(u_N)\delta v_N &= na\Delta\delta\bar{i}_x \\ (\sin(u_N) + \tfrac{2\kappa T}{n+\kappa(\eta P+Q)}(u_f - u_N)\cos(u_N))\delta v_N &= na\Delta\delta\bar{i}_y \end{aligned} \tag{24}$$

which shows that in the presence of $J_2$ effects, $\delta i_y$ drifts linearly with time and proportionally to $\delta i_x$. Since the latter is in general affected by the maneuver, the change in drift of $\delta i_y$ needs to be taken into account for precision. The single impulse magnitude is derived from the first of Eq. 24 as

$$\delta v_N = na\frac{\Delta\delta\bar{i}_x}{\cos(u_N)} \tag{25}$$

The impulse location is found by dividing the second by the first expression of Eq. 24 to find the following transcendental equation

$$\tan(u_N) + \frac{2\kappa T}{n+\kappa(\eta P+Q)}(u_f - u_N) = \frac{\Delta\delta\bar{i}_y}{\Delta\delta\bar{i}_x} \tag{26}$$

Although Eq. 26 yields no analytical solution, Eq. 23 provides a good initial guess for an iterative approach. In practice, only one iteration is sufficient to find the optimal maneuver location which takes into account $J_2$ effects properly. Once the location of the cross-track maneuver is computed, the corresponding $\delta v_N$ can be found by direct substitution in Eq. 25. Table 2 summarizes the results of this section.

Table 2: Summary of optimal out-of-plane impulsive maneuvers in near-circular orbits

| $J_2$ effects included | Type of solution | Location of maneuver |
|---|---|---|
| No | Analytical | $u_{ideal} = \arctan(\frac{\Delta\delta i_y}{\Delta\delta i_x})$ |
| Yes | Iterative | Initialization: $\tan(u_N) = \frac{2\kappa T}{n+\kappa(\eta P+Q)}(u_f - u_{ideal}) = \frac{\Delta\delta\bar{i}_y}{\Delta\delta\bar{i}_x}$ Iterations: $\tan(u_N^+) + \frac{2\kappa T}{n+\kappa(\eta P+Q)}(u_f - u_N^-) = \frac{\Delta\delta\bar{i}_y}{\Delta\delta\bar{i}_x}$ |

The benefit of this solution over earlier approaches is more evident over longer control windows and when the x-component of the relative inclination vector is changed substantially earlier in the reconfiguration.

### B. In-Plane Reconfiguration

Similar to the out-of-plane control problem, this section applies Earth's oblateness $J_2$ effects throughout the complete reconfiguration as potentially affected by each intermediate along-track maneuver. As discussed in Sec. III, three tangential maneuvers are considered as potential candidates capable of achieving the delta-v lower bound for an arbitrary reconfiguration. From Eq. 8 and 10, the evolution of the in-plane ROE is governed by

$$\begin{gathered} 2(\delta v_{T1} + \delta v_{T2} + \delta v_{T3}) = na\Delta\delta\bar{a} \\ -q\delta v_{T1} - p\delta v_{T2} - l\delta v_{T3} = na\Delta\delta\bar{\lambda} \\ 2\cos(U_1)\delta v_{T1} + 2\cos(U_2)\delta v_{T2} + 2\cos(U_3)\delta v_{T3} = na\Delta\delta\bar{e}_x \\ 2\sin(U_1)\delta v_{T1} + 2\sin(U_2)\delta v_{T2} + 2\sin(U_3)\delta v_{T3} = na\Delta\delta\bar{e}_y \end{gathered} \tag{27}$$

where

$$\begin{gathered} q = (u_f - u_{T1} - \tfrac{c}{1-c}u_f) \\ p = (u_f - u_{T2} - \tfrac{c}{1-c}u_f) \\ l = (u_f - u_{T3} - \tfrac{c}{1-c}u_f) \\ U_i = (1-c)u_{Ti} + cu_f \\ c = \tfrac{\dot{\omega}}{n+\kappa(\eta P+Q)} \end{gathered} \tag{28}$$

It is noted that the effects of a cross-track maneuver executed during the reconfiguration interval $[u_0, u_f]$ can be incorporated in the computation of $\Delta\delta\bar{\lambda}$ without loss of generality. The expressions for the variation of the relative eccentricity vector in the presence of $J_2$ effects (i.e., the last two of Eq. 27) has been derived by considering the following convenient form for the evolution of $\delta\boldsymbol{e}$ subject to three tangential impulses

$$\boldsymbol{R}_{f,3}(\boldsymbol{R}_{3,2}(\boldsymbol{R}_{2,1}(\boldsymbol{R}_{1,0}\delta\boldsymbol{e}_0 + \Delta\delta\boldsymbol{e}_1) + \Delta\delta\boldsymbol{e}_2) + \Delta\delta\boldsymbol{e}_3) = \delta\boldsymbol{e}_f \tag{29}$$

where $\boldsymbol{R}_{j,i}$ is the rotation matrix applied to $\delta\boldsymbol{e}$ between arguments of latitude $u_i$ and $u_j$ according to

$$\boldsymbol{R}_{j,i} = \begin{bmatrix} \cos(c(u_j - u_i)) & -\sin(c(u_j - u_i)) \\ \sin(c(u_j - u_i)) & \cos(c(u_j - u_i)) \end{bmatrix} \tag{30}$$

and $\Delta\delta\boldsymbol{e}_i$ represent the change of the relative eccentricity vector caused by a tangential burn at location $u_i$. It is remarkable that Eq. 27 retains the same form of the equivalent expressions for the un-perturbed near-circular case.[10] This is obvious when substituting $J_2 = 0$ in Eq. 28. As a consequence, the structural solution is identical and the maneuver locations can be obtained through a change variable as

$$u_{Ti} = \frac{1}{1-c}(\arctan(\frac{\Delta\delta\bar{e}_y}{\Delta\delta\bar{e}_x}) + k_i\pi - cu_f) \tag{31}$$

whereas the maneuver delta-v sizes are listed in Tables 3 and 4. In the unperturbed case, the optimal maneuvers occur at multiples of half the orbital period $k_i\pi$ from an initial maneuver location which corresponds to the phase of the total desired variation of the relative eccentricity vector

$$\bar{U} = \arctan(\frac{\Delta\delta\bar{e}_y}{\Delta\delta\bar{e}_x}) \tag{32}$$

In the newly addressed perturbed case, the maneuver locations are slightly shifted due to the mean $J_2$ effects acting on the argument of perigee which are captured by the coefficient $c$.

Table 3 can be used to compute the magnitudes of the three delta-v maneuvers for a given reconfiguration. Suppose that the desired change in ROE is given by

$$\begin{bmatrix} a\Delta\delta\bar{a} & a\Delta\delta\bar{\lambda} & a\Delta\delta\bar{e_x} & a\Delta\delta\bar{e_y} \end{bmatrix} = \begin{bmatrix} -20 & 200 & -80 & 50 \end{bmatrix} \text{ m} \tag{33}$$

after pre-compensation of the perturbations acting between the given initial and final conditions of the reconfiguration (see Eq. 15). Then $\bar{U}$ is calculated via Eq. 32 to be 2.5830 rad, which represents the phase of the desired variation of the relative eccentricity vector. Because $\bar{U} \in [\frac{\pi}{2}, \pi]$, B, b, $k_i$, and g are defined according to the last row of Table 3. If the maneuvers are chosen to occur at $k_1 = 0$, $k_2 = 1$, and $k_3 = 14$, then $\text{sign}(\cos U_1) = (+)$, $\text{sign}(\cos U_2) = (-)$, and $\text{sign}(\cos U_3) = (+)$, which corresponds to $g = -1$. The set of derived signs corresponds to $\delta v_{T1}$ and $\delta v_{T3}$ calculated according to the expressions in the last column of Table 4, using $\Delta\delta\lambda'$ (defined in Eq. 34), whereas $\delta v_{T2} = \delta v_T$ as defined in first row of Table 3. Finally, the maneuver locations $u_{Ti}$ are calculated via Eq. 31 using the chosen $k_i$.

Table 3: Closed-form delta-v solutions for in-plane reconfiguration in perturbed near-circular orbits

| Aimed end-conditions | | | $k_i$ | $\delta v_T = na\frac{b\Delta\delta\bar{a}+gB}{4b}$ | |
|---|---|---|---|---|---|
| | $B$ | $b$ | Signs | $(+,-,-),(-,-,+),(-,+,-)$ | $(+,-,+),(+,+,-),(-,+,+)$ |
| $\bar{U} \in [0, \frac{\pi}{2}]$ | $\Delta\delta\bar{e}_x$ | $\cos\bar{U}$ | $\text{sign}\cos U_i$ | $g = 1$ | $g = -1$ |
| $\bar{U} = \frac{\pi}{2}$ | $\Delta\delta\bar{e}_y$ | $\sin\bar{U}$ | $\text{sign}\sin U_i$ | $g = 1$ | $g = -1$ |
| $\bar{U} \in [\frac{\pi}{2}, \pi]$ | $\Delta\delta\bar{e}_x$ | $\lvert\cos\bar{U}\rvert$ | $\text{sign}\cos U_i$ | $g = -1$ | $g = 1$ |

Table 4: $\delta v$ Computation

| Signs | $\delta v_T$ | $D$ | $\delta v$ expressions |
|---|---|---|---|
| $(+,-,-)$ | $\delta v_{T1}$ | $12b(p-l)$ | $\delta v_{T2} = -na(4b\Delta\delta\bar{\lambda}' + 3g(q-l)B + 3b(q+l)\Delta\delta\bar{a})/D$ |
| $(-,+,+)$ | | | $\delta v_{T3} = +na(4b\Delta\delta\bar{\lambda}' + 3g(q-p)B + 3b(q+p)\Delta\delta\bar{a})/D$ |
| $(-,-,+)$ | $\delta v_{T3}$ | $12b(q-p)$ | $\delta v_{T1} = -na(4b\Delta\delta\bar{\lambda}' - 3g(p-l)B + 3b(p+l)\Delta\delta\bar{a})/D$ |
| $(+,+,-)$ | | | $\delta v_{T2} = +na(4b\Delta\delta\bar{\lambda}' - 3g(q-l)B + 3b(q+l)\Delta\delta\bar{a})/D$ |
| $(-,+,-)$ | $\delta v_{T2}$ | $12b(q-l)$ | $\delta v_{T1} = -na(4b\Delta\delta\bar{\lambda}' + 3g(p-l)B + 3b(p+l)\Delta\delta\bar{a})/D$ |
| $(+,-,+)$ | | | $\delta v_{T3} = na(4b\Delta\delta\bar{\lambda}' - 3g(q-p)B + 3b(q+p)\Delta\delta\bar{a})/D$ |

where

$$\Delta\delta\bar{\lambda}' = \frac{n + \kappa(\eta P + Q)}{n}\Delta\delta\lambda + \frac{3}{2}\frac{c}{1-c}u_f\Delta\delta a \tag{34}$$

As for the unperturbed case, this solution is optimal when the reconfiguration cost is driven by the variation of relative eccentricity vector, i.e. $||\Delta\delta\bar{\boldsymbol{e}}|| \geq |\Delta\delta\bar{a}|$ and $||\Delta\delta\bar{\boldsymbol{e}}|| \geq |\Delta\delta\bar{\lambda}|/(\frac{3}{2}\Delta M)$. The benefit of this solution as compared with previous approaches is more evident for larger control windows and for larger effects of $J_2$ on the argument of perigee (small inclinations). An analytical solution for the cases of dominant $|\Delta\delta\bar{a}|$ or $|\Delta\delta\bar{\lambda}|$ is not available yet and should prioritize maneuver locations which provide a minimum path length in the evolution of $\delta a$ during the reconfiguration.

# VI. Control in Unperturbed Eccentric Orbits

## A. Out-of-Plane Reconfiguration

No closed-form solution is available in literature for out-of-plane control in eccentric orbits, however the derivation is trivial within the framework outlined in this paper. Ignoring $J_2$ effects, the dynamics of the relative inclination vector are given by Eq. 13 as

$$\begin{aligned} \eta\delta v_N \tfrac{\cos(\theta_N)}{1+e\cos(\nu_N)} &= \Delta\delta\bar{i}_x \\ \eta\delta v_N \tfrac{\sin(\theta_N)}{1+e\cos(\nu_N)} &= \Delta\delta\bar{i}_y \end{aligned} \tag{35}$$

Evidently, one cross-track maneuver is necessary and sufficient to accomplish an arbitrary reconfiguration. The maneuver location is given by dividing the second by the first of Eq. 35, whereas the maneuver magnitude is given by adding the squares of the two expressions as follows

$$\begin{aligned} \theta_N &= \arctan(\tfrac{\Delta\delta\bar{i}_y}{\Delta\delta\bar{i}_x}) \\ |\delta v_N| &= na\tfrac{1+e\cos(\theta_N)}{\sqrt{1-e^2}}||\Delta\delta\bar{\boldsymbol{i}}|| \end{aligned} \tag{36}$$

Similar to the near-circular case, the maneuver is located at the phase of the variation of the relative inclination vector, now represented by a true argument of latitude though $\theta_N = \nu_N + \omega_N$. The maneuver size is proportional to the length of the variation of the relative inclination vector, however it is also a function of the maneuver location in eccentric orbits. In particular, the delta-v is maximum for maneuvers executed at the equator and minimum for maneuvers executed at the extreme northern or southern latitudes.

## B. In-Plane Reconfiguration

No closed-form is available in literature for in-plane control in eccentric orbits. Here, similar to Sec. V.B, an optimal semi-analytical solution is derived for reconfigurations where $||\Delta\delta\bar{\boldsymbol{e}}|| \geq |\Delta\delta\bar{a}|\frac{\eta^2}{1+e}$ and $||\Delta\delta\bar{\boldsymbol{e}}|| \geq |\Delta\delta\bar{\lambda}|\frac{2\eta^2}{3(1+e)\Delta M}$. This generalizes previous work done in near-circular orbits. As discussed in Sec. III, three tangential maneuvers are considered as potential candidates capable of achieving the delta-v lower bound for an arbitrary reconfiguration. Neglecting $J_2$ effects, from Eq. 12 and 13, the evolution of the in-plane ROE is governed by

$$\begin{aligned} (1+e\cos(\nu_1))\delta v_{T1} + (1+e\cos(\nu_2))\delta v_{T2} + (1+e\cos(\nu_3))\delta v_{T3} &= \tfrac{\eta na\Delta\delta\bar{a}}{2} \\ -(1+e\cos(\nu_1))\Delta M_{f1}\delta v_{T1} - (1+e\cos(\nu_2))\Delta M_{f2}\delta v_{T2} - (1+e\cos(\nu_3))\Delta M_{f3}\delta v_{T3} &= \tfrac{\eta na\Delta\delta\bar{\lambda}_e}{3} \\ \tfrac{(2+e\cos(\nu_1))\cos(\theta_1)+e_x}{1+e\cos(\nu_1)}\delta v_{T1} + \tfrac{(2+e\cos(\nu_2))\cos(\theta_2)+e_x}{1+e\cos(\nu_2)}\delta v_{T2} + \tfrac{(2+e\cos(\nu_3))\cos(\theta_3)+e_x}{1+e\cos(\nu_3)}\delta v_{T3} &= \tfrac{na\Delta\delta\bar{e}_x}{\eta} - \tfrac{e_y na\Delta\delta\bar{i}_y}{\eta\tan(i)} \\ \tfrac{(2+e\cos(\nu_1))\sin(\theta_1)+e_y}{1+e\cos(\nu_1)}\delta v_{T1} + \tfrac{(2+e\cos(\nu_2))\sin(\theta_2)+e_y}{1+e\cos(\nu_2)}\delta v_{T2} + \tfrac{(2+e\cos(\nu_3))\sin(\theta_3)+e_y}{1+e\cos(\nu_3)}\delta v_{T3} &= \tfrac{na\Delta\delta\bar{e}_y}{\eta} + \tfrac{e_x na\Delta\delta\bar{i}_y}{\eta\tan(i)} \end{aligned} \tag{37}$$

where $\Delta M_{ij} = M_i - M_j$. Inverting the first three of Eq. 37, the following analytical solution is found

$$\begin{aligned} \delta v_{T1} &= na\tfrac{h_{23}}{K_{123}} \\ \delta v_{T2} &= -na\tfrac{h_{13}}{K_{123}} \\ \delta v_{T3} &= na\tfrac{h_{12}}{K_{123}} \end{aligned} \tag{38}$$

where

$$
\begin{gathered}
K_{ijk} = 6\eta\tan(i)(\Delta M_{ij} f_i f_j g_k + \Delta M_{ki} f_i f_k g_j + \Delta M_{jk} f_j f_k g_i) \\
h_{ij} = 2\Delta\delta\bar{\lambda}_e \eta^2 (f_i g_j - f_j g_i) + 6\Delta M_{ij} f_i f_j (\Delta\delta\bar{e}_x \tan(i) - \Delta\delta\bar{i}_y e_y) + 3\Delta\delta\bar{a}\eta^2 \tan(i)(\Delta M_{fi} f_i g_j - \Delta M_{fj} f_j g_i) \\
f_i = 1 + e\cos(\nu_i) \\
g_i = [(1+f_i)\cos(\theta_i) + e_x]/f_i
\end{gathered}
\tag{39}
$$

Each maneuver size given by Eq. 38 and 39 depends on the unknown location of the maneuver. The locations that minimize the total delta-v, or equivalently our merit functional $J_{ctrl}$, must satisfy the last of Eq. 37. In addition, for reconfigurations where $||\Delta\delta\bar{\mathbf{e}}||$ is dominant, the maneuvers must ensure a minimum path when connecting the initial and final relative eccentricity vectors. In the absence of perturbations, this means that the individual corrections of the relative eccentricity vector must be collinear. Thus, from Eq. 13, the following must hold for each maneuver

$$
\begin{gathered}
\frac{(2+e_x\cos(\theta_i)+e_y\sin(\theta_i))\cos(\theta_i)+e_x}{1+e_x\cos(\theta_i)+e_y\sin(\theta_i)}\delta v_T/na = \frac{\Delta\delta\bar{e}_x}{\eta} - \frac{e_y\Delta\delta\bar{i}_y}{\eta\tan(i)} \\
\frac{(2+e_x\cos(\theta_i)+e_y\sin(\theta_i))\sin(\theta_i)+e_y}{1+e_x\cos(\theta_i)+e_y\sin(\theta_i)}\delta v_T/na = \frac{\Delta\delta\bar{e}_y}{\eta} + \frac{e_x\Delta\delta\bar{i}_y}{\eta\tan(i)}
\end{gathered}
\tag{40}
$$

Dividing the second by the first of Eq. 40 gives the following relationship for the true argument of latitude $\theta_i$ of the maneuvers

$$
\tan(\theta_i)\frac{1+\frac{e_y}{(2+e_x\cos(\theta_i)+e_y\sin(\theta_i))\sin(\theta_i)}}{1+\frac{e_x}{(2+e_x\cos(\theta_i)+e_y\sin(\theta_i))\cos(\theta_i)}} = \frac{\Delta\delta\bar{e}_y\tan(i) + e_x\Delta\delta\bar{i}_y}{\Delta\delta\bar{e}_x\tan(i) - e_y\Delta\delta\bar{i}_y}
\tag{41}
$$

The resulting formula for the optimal maneuver locations is a non-linear function of the unknowns that can not be solved analytically. On the other hand, Eq. 41 reduces to a very simple form for $e = 0$ that admits the well-known analytical solution

$$
\theta_i = \arctan\left(\frac{\Delta\delta\bar{e}_y}{\Delta\delta\bar{e}_x}\right) + k_i\pi
\tag{42}
$$

with $k_i$ being a natural number. Equation 42 can be used as a good initial guess to efficiently solve for the optimal maneuver locations in eccentric orbits given by Eq. 41 in at most six iterations. It is noteworthy that the choice of integers $k_i$ allows to arbitrarily select maneuver locations among the infinite available solutions, thus simplifying the compliance with operational constraints.

## VII. Analogy between Absolute and Relative Orbit Control

It is possible to establish a strong analogy between absolute and relative orbit control by considering the simultaneous effects of an impulsive maneuver on the absolute orbit elements of the deputy (or active) spacecraft and on the relative orbit elements with respect to the chief (or passive) spacecraft. For example, the variations of ROE caused by a maneuver can be expressed as

$$
\begin{gathered}
a\Delta\delta a = a\delta a^+ - a\delta a^- = (a_d - a)^+ - (a_d - a)^- = \Delta a_d \\
\Delta\delta\boldsymbol{e} = \delta\boldsymbol{e}^+ - \delta\boldsymbol{e}^- = (\boldsymbol{e}_d - \boldsymbol{e})^+ - (\boldsymbol{e}_d - \boldsymbol{e})^- = \Delta\boldsymbol{e}_d
\end{gathered}
\tag{43}
$$

where the superscripts $-$ and $+$ indicate quantities before and after the impulsive maneuver respectively, and the symbol $\Delta = ()^+ - ()^-$ indicate arithmetic differences of quantities after and before the maneuver. It is evident that the variation of ROE caused by a maneuver is equivalent to a variation of absolute orbit elements caused by the same maneuver. Usually the latter is referred to as absolute orbit control, whereas the former is relative orbit control. Since optimal closed-form solutions for absolute orbit control exist (e.g., Hohmann transfer), it is legitimate to compare those solutions with the ones used for relative orbit control to verify optimality and improve our understanding of the control problem. In particular, the elliptic Hohmann transfer[38] has been shown to be fuel-optimal for the small corrections of semi-major axis and eccentricity considered in this paper, i.e. $\Delta a_d/a_d << 1$ and $\Delta e_d/e_d << 1$. Re-casting the elliptic Hohmann transfer as a relative orbit control problem and applying the linearization assumptions used in this work should provide a solution consistent with our methodology.

Consider the problem of absolute orbit transfer using minimum energy from an initial elliptic orbit $(a, e)$ to a final target elliptic orbit $(a + \Delta a, e + \Delta e)$ with $\Delta a/a << 1$ and $\Delta e/e << 1$. No specific changes of argument of perigee (phase of eccentricity vector) or mean argument of latitude (or mean longitude) are prescribed. Further, let the transfer orbit be characterized by $(a + \Delta a^*, e + \Delta e^*)$. Exploiting the ellipse's geometry (see Fig. 4), the relationship between $\Delta()$ and $\Delta()^*$ is given by

$$\begin{array}{c} \Delta a^* = \frac{a\Delta e}{2} + (1+e)\frac{\Delta a}{2} + \Delta a \Delta e \\ \Delta e^* = \frac{(1-e)\Delta a^*}{a+\Delta a^*} \end{array} \tag{44}$$

Neglecting second order terms of the type $\Delta()\Delta()$, after substitution of the first into the second of Eq. 44, yields

$$\begin{array}{c} \Delta a^* \approx \frac{a\Delta e}{2} + (1+e)\frac{\Delta a}{2} \\ \Delta e^* \approx \frac{(1-e)\Delta e}{2} + \frac{(1-e^2)\Delta a}{2a} \end{array} \tag{45}$$

According to the Hohmann transfer illustrated in Fig. 4, the transfer orbit is tangent to the initial and final orbits at the line of apses.

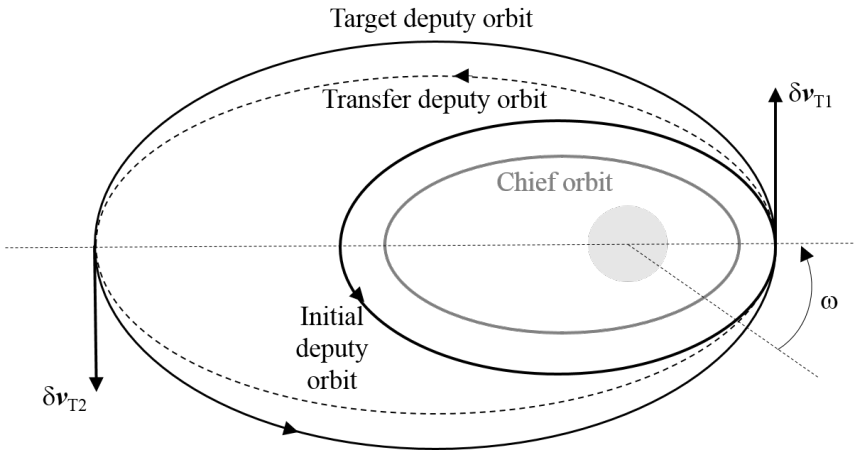


Figure 4: Notional illustration of elliptic Hohmann transfer as applied to relative orbit control. The deputy spacecraft is active and performs two tangential maneuvers at the line of apses to change semi-major axis and eccentricity with minimum fuel consumption.

A first tangential maneuver is executed at the periapsis of the initial orbit, $\nu_1 = 0$, which is obtained from the difference of velocities on the transfer and initial orbits as

$$\delta v_{T1} = \sqrt{\frac{2\mu}{(a+\Delta a^*)(1-e-\Delta e^*)} - \frac{\mu}{a+\Delta a^*}} - \sqrt{\frac{2\mu}{a(1-e)} - \frac{\mu}{a}} \tag{46}$$

This expression can be simplified without approximations to

$$\delta v_{T1} = \sqrt{\frac{\mu}{a}\frac{1+e}{1-e}}\sqrt{\frac{1}{1+\frac{\Delta a^*}{a}}}\sqrt{\frac{1+\frac{\Delta e^*}{1+e}}{1+\frac{\Delta e^*}{1-e}}} \tag{47}$$

Substitution of Eq. 44 into Eq. 47 provides an explicit expression of the maneuver size as a function of the total desired variations of orbit elements. However, in the case of small corrections, $\Delta()$, a Taylor expansion of the square roots $(1 + \Delta())^{0.5}$ can be conveniently truncated to first order as $(1 + 0.5\Delta())$, resulting in the following simple expression

$$\delta v_{T1} \approx \sqrt{\frac{\mu}{a}\frac{1+e}{1-e}}\frac{\Delta a^*}{2a} \approx \frac{1}{4}\sqrt{\frac{\mu}{a}\frac{1+e}{1-e}}[(1+e)\frac{\Delta a}{a} + \Delta e] \tag{48}$$

The second tangential maneuver of the Hohmann transfer is executed at the apoapsis of the transfer orbit (which is the orbit of the maneuvering spacecraft), $\nu_2 = \pi$, and can be derived similarly to the first maneuver as

$$\delta v_{T2} \approx \sqrt{\frac{\mu}{a}\frac{1+e}{1-e}}\frac{\Delta a^*}{2a} \approx \frac{1}{4}\sqrt{\frac{\mu}{a}\frac{1+e}{1-e}}[(1-e)\frac{\Delta a}{a} - \Delta e] \tag{49}$$

Considering the equivalence between absolute and relative orbit corrections formalized by Eq. 43, Eq. 48 and 49 represent an optimal closed-form solution for relative orbit control in the special case that only the relative semi-major axis and the magnitude of the relative eccentricity vector (initially aligned with the absolute eccentricity vector) are to be corrected. In this case, according to our problem definition and the delta-v lower bound, two tangential maneuvers can guarantee minimum fuel consumption. For near-circular orbits, this solution matches the well-known double-impulse maneuvering scheme adopted in previous flight demonstrations such as SAFE,[2] TAFF,[3] and ARGON.[5] In fact, besides having the same delta-v size, the two maneuvers are separated by half an orbit revolution and the location of the first maneuver is at the phase of the variation of the relative eccentricity vector (here the line of apses). For eccentric orbits, if the desired variation of the eccentricity vector is aligned with the argument of periapsis, i.e. $\arctan(\Delta\delta e_y/\Delta\delta e_x) = \omega$, Eq. 41 reduces to $\nu_i = k_i\pi$, with $k_i$ being an integer number. This ensures a minimum path for the relative eccentricity vector. Substituting these maneuver locations in Eq. 37 and neglecting the variation of $\delta\lambda_e$ over the course of the reconfiguration, provides two equations in the two unknown maneuver sizes. The solution of these equations matches Eq. 48 and 49 identically. This conclusion verifies the optimal nature of the approach used in this paper. In addition, the fact that the elliptic Hohmann transfer is also optimal for variations $|\Delta a/a| > |\Delta e|$ suggests that our closed-form optimal solution for formation-flying in elliptic orbits is also optimal for dominant variations of relative semi-major axis when absolute and relative eccentricity vectors are collinear.

## VIII. Numerical Validation

The new four (semi-)analytical fuel-optimal impulsive control schemes derived in this paper are validated in this section. A numerical integration of the nonlinear equations of motion including Earth's oblateness $J_2$ effects is used to verify the capability of the control solutions to reconfigure the formation as prescribed. An optimization algorithm based on primer vector theory is used as benchmark to evaluate the optimality of the solutions in terms of delta-v.

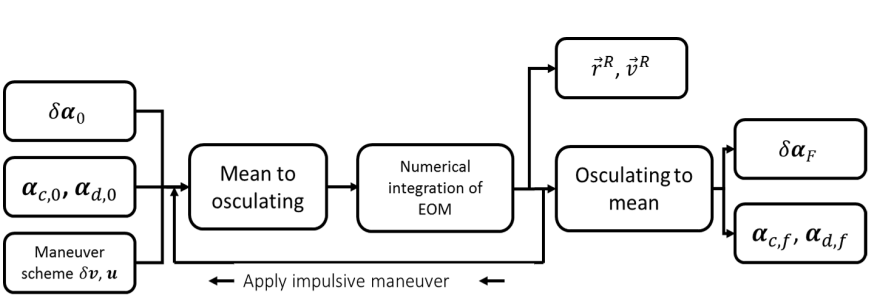


(a) Overall simulation architecture

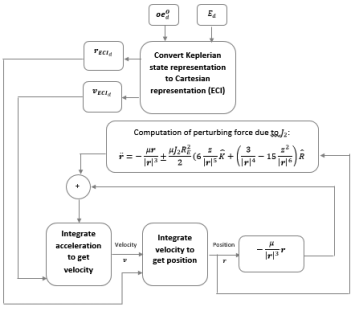


(b) Numerical integration of the equations of motion

Figure 5: Numerical integration scheme

As illustrated in Fig. 5, the numerical integration is conducted in the Earth Centered Inertial (ECI) frame and generates position and velocity of the chief and deputy spacecraft. The nonlinear equations of motion are initialized using osculating orbit elements which are derived from the prescribed mean orbit elements using the linear transformations developed by Schaub,[15] first order in $J_2$. Impulsive maneuvers are computed in the RTN frame based on the new solutions developed in this paper using as input the initial and final desired mean ROE. The resulting delta-v's are then rotated to ECI and added as discontinuities to the velocity of the deputy spacecraft. After the simulation, the actually achieved and desired mean ROE

are compared to determine the accuracy of the reconfiguration. The overall simulation scheme is illustrated in Fig. 5(a), whereas Fig 5(b) provides a detail of the numerical integration block.

The optimal control algorithm used as reference has been designed by Roscoe et al.[19] Based on Pontryagin's minimum principle, it iteratively solves the discrete-time optimal control problem and refines the solution using Lawden's primer vector theory.[20] In particular, the primer vector history $p(t)$ associated with the maneuvering scheme output by the discrete-time optimal solution is used to decide whether to add, remove, or move impulsive maneuvers so to converge towards the continuous-time optimal solution. The adopted criteria for the correction of a tentative solution is summarized by the following conditions[19]

1. If $\dot{p}(t) \neq 0$ at the time of any impulse, move the impulse slightly in the direction of increasing $p$ ($\dot{p} > 0$)
2. If $p(t) > 1$ somewhere other than in the vicinity of an impulse, add another impulse at the time of maximum $p(t)$
3. If $p(t) < 1$ and $\dot{p}(t) = 0$ at the time of any impulse, remove that impulse

In order to ensure consistency with the solutions found in this paper, the primer vector algorithm uses the STM from Eq. 8 for near-circular perturbed orbits and the STM from Eq. 12 for unperturbed eccentric orbits. Although the output of this algorithm is the truly optimal impulsive maneuver sequence, it suffers from high computational effort and poor convergence properties, and is only used for comparison in the following. In order to highlight the strengths and weaknesses of the (semi-)analytical optimal control solutions, four test cases are defined for perturbed near-circular orbits and three test cases for unperturbed eccentric orbits.

In particular, Tests 1-3 address in-plane control using the solutions from Tables 3-4, whereas Test 4 addresses out-of-plane control using the solution from Eqs. 25 and 26. In contrast to previous work in near-circular orbits, these solutions are derived using a STM $\bar{\mathbf{\Phi}}$ from Eq. 8 which incorporates $J_2$ effects. To show the benefits of this approach, the Tests 1-4 are defined to amplify the effects of $J_2$ during the reconfiguration that can not be captured by a simple pre-compensation of the total desired variation of ROE (see Eq. 15) based on the initial conditions. Since the presented in-plane control solutions are only optimal for dominant $||\Delta\delta\bar{\boldsymbol{e}}||$, Test 3 increases gradually the desired change in relative semi-major axis until $|\Delta\delta\bar{a}| > ||\Delta\delta\bar{\boldsymbol{e}}||$. A comparison with the optimal solutions from primer vector theory shows how the (semi-)analytical maneuvering scheme becomes suboptimal in this case.

Similarly, Tests 5-7 are designed to evaluate unperturbed eccentric orbits. In particular, Test 5-6 address in-plane control using the solution from Eqs. 38-42, whereas Test 7 addresses out-of-plane control using the solution from Eq. 36. The optimality of each reconfiguration is evaluated through a comparison with the results from primer vector theory.

## A. In-Plane Control in Perturbed Near-Circular Orbits

### *1. Test 1: Dominant $||\Delta\delta\bar{\boldsymbol{e}}||$, High drift rate of reference argument of perigee*

As discussed in Section III, previous work takes into account perturbations during the reconfiguration interval in the guidance layer by subtracting the effects of these perturbations (e.g., $J_2$, differential drag) from the target desired ROE. As shown by Eq. 15, this so-called pre-compensation results in a total desired change of ROE given by $\Delta\delta\bar{\boldsymbol{\alpha}} = \delta\boldsymbol{\alpha}_f - \mathbf{\Phi}_{f,0}\delta\boldsymbol{\alpha}_0$, where the initial and final ROE are given and the STM is used for propagation. Tests 1, 2, and 4 show that such pre-compensation is not sufficient to obtain accurate results when the variations of perturbations caused by the change of ROE during the reconfiguration due to the maneuver themselves are not taken into account. The new maneuver solutions are derived from a more accurate $\bar{\mathbf{\Phi}}$, i.e. Eq. 8, and take these effects into account. The drift in the reference argument of perigee is given by

$$\dot{\omega} = \frac{3}{4}\frac{J_2 R_e^2 \sqrt{\mu}}{a^{7/2}\eta^4}(5\cos i^2 - 1) \tag{50}$$

and is highest when the chief orbit is equatorial and its semi-major axis is small. As a consequence, we select the chief orbit elements to be

$$\boldsymbol{\alpha}_{c,0} = \begin{bmatrix} 6578 \text{ km} & 0 & 8^o & 0 & 0 & 0 \end{bmatrix} \tag{51}$$

which correspond to a low Earth near-equatorial orbit. The reconfiguration parameters are selected as

$$
\begin{aligned}
a\delta\boldsymbol{\alpha}_0 &= \begin{bmatrix} 30 & -11000 & 0 & -50 & 0 & 0 \end{bmatrix} \text{ m} \\
a\delta\boldsymbol{\alpha}_f &= \begin{bmatrix} 0 & -10500 & 45 & 70 & 0 & 0 \end{bmatrix} \text{ m} \\
\Delta u &= 5 \text{ orbits}
\end{aligned}
\tag{52}
$$

which correspond to a variation of all in-plane ROE within five orbits. After pre-compensation, the desired variations of ROE are such that $||\Delta\delta\bar{\boldsymbol{e}}||$ is the dominant correction among all in Eq. 22 and

$$
a\Delta\delta\bar{\boldsymbol{\alpha}} = \begin{bmatrix} -30 & 1907.4 & 40.3 & 119.8 & 0 & 0 \end{bmatrix} \text{ m} \tag{53}
$$

The evolution of the ROE after application of the new semi-analytical maneuver sequence given in Tables 3-4 is illustrated in Fig. 6. In particular, the relative eccentricity vector is shown in Fig. 6(a), whereas the relative semi-major axis and relative mean longitude in Fig. 6(b). The locations of the maneuvers are tagged by the letters B1, B2, and B3, whereas $-$ and $+$ are used to indicate the state right before and after a maneuver. Stylized straight lines starting from the origin represent the relative eccentricity vector. Note that the impulsive maneuvers do not connect the tips of the relative eccentricity vectors. This is because the $J_2$ effects are taken into account, which in this case help reducing the delta-v budget. In other cases, the drift due to $J_2$ may hinder the reconfiguration, thus increasing the cost. Overall this represents a minimum path solution in the ROE space which is deformed by perturbations.

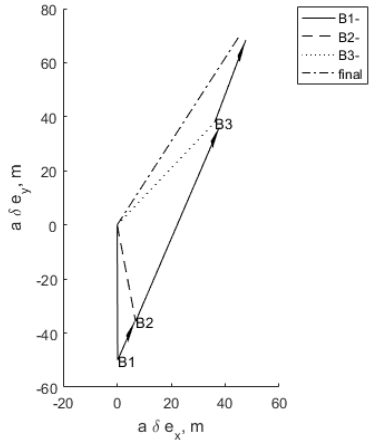


(a) Relative eccentricity vector as affected by maneuvers (arrows) and natural perturbations.

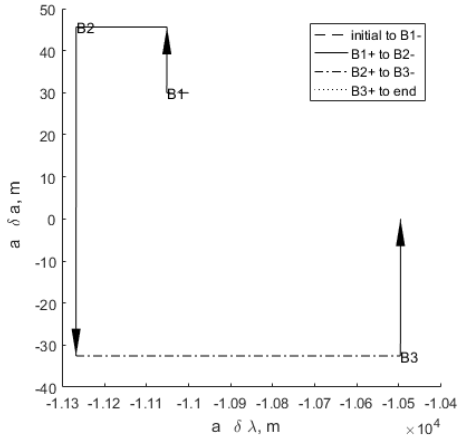


(b) Relative semi-major axis and relative mean longitude as affected by maneuvers (arrows) and natural perturbations.

Figure 6: Evolution of ROE in Test 1 in the presence of $J_2$ effects

Table 5 shows a comparison between the accuracy of the new semi-analytical solution given by Tables 3-4 and previous solutions which do not take into account the effects of $J_2$ besides the pre-compensation.[10] Due to the significant precession of the argument of perigee, the maneuver locations are slightly shifted in time, leading to a substantial reduction of the reconfiguration error in relative terms.

Table 5: Reconfiguration accuracy comparison for Test 1

| ROE | Desired ROE, m | Achieved ROE, $J_2 = 0$ | Relative error | Achieved ROE, $J_2$ | Relative error |
|---|---|---|---|---|---|
| $\delta a$ | 0 | 0 | 0% | 0 | 0% |
| $\delta\lambda$ | -10500 | -10498.39 | 0.015% | -10495.98 | 0.038% |
| $\delta e_x$ | 45 | 41.52 | 7.73% | 45.30 | 0.068% |
| $\delta e_y$ | 70 | 72.93 | 4.18% | 69.90 | 0.15% |

Table 6: Comparison of maneuver schemes calculated using primer vector and semi-analytical solutions

| $k_i$ (maneuver locations) | Primer vector theory | Semi-analytical solution |
|---|---|---|
| 0 | $0.0092\frac{m}{s}$ | $0.0092\frac{m}{s}$ |
| 1 | $-0.0463\frac{m}{s}$ | $-0.0463\frac{m}{s}$ |
| 6 | $0.0193\frac{m}{s}$ | $0.0194\frac{m}{s}$ |
| Total delta-v | $0.0749\frac{m}{s}$ | $0.0748\frac{m}{s}$ |

The semi-analytical solution meets the delta-v lower bound of $0.0748\frac{m}{s}$ calculated using Eq. 22 and is thus optimal. To further confirm this, Table 6 shows a comparison of the (semi-)analytical solution with the output obtained by the primer vector optimal control algorithm. More details on the iterative process used to generate the primer vector theory based solutions are provided in Section IXA. As demonstrated in Table 6, the quasi-analytical maneuvering scheme is indeed optimal.

### *2. Test 2: Dominant $||\Delta\delta\bar{\boldsymbol{e}}||$, Long reconfiguration*

Similar to Test 1, here it is shown that pre-compensating perturbations in the guidance layer is not accurate enough for long reconfigurations. The same chief reference initial orbit from Eq. 51 is employed, whereas the new reconfiguration parameters are given by

$$\begin{aligned} a\delta\boldsymbol{\alpha}_0 &= \begin{bmatrix} 60 & -11000 & 0 & 50 & 0 & 0 \end{bmatrix} \text{ m} \\ a\delta\boldsymbol{\alpha}_f &= \begin{bmatrix} 0 & -10500 & 150 & -50 & 0 & 0 \end{bmatrix} \text{ m} \\ \Delta u &= 28 \text{ orbits} \end{aligned} \tag{54}$$

which result in the following required variations of ROE after pre-compensation

$$a\Delta\delta\bar{\boldsymbol{\alpha}} = \begin{bmatrix} -60 & 16263.3 & 174.9 & -93.3 & 0 & 0 \end{bmatrix} \text{ m} \tag{55}$$

In the presence of $J_2$, the relative eccentricity vector and the absolute eccentricity vector both rotate at an angular rate given by Eq. 50. Given the initial orbital elements of the chief, the angular rate amounts to $(-2.02 \times 10^{-4})^o/s$. This yields a full rotation of the eccentricity vector in about 21 days. If this effect was not taken into account in the computation of the maneuver locations, significant errors in the achieved ROE would occur. To show this, a long reconfiguration interval of 28 orbits is adopted. This corresponds to 1.75 days and a drift in the eccentricity vector of about $30^o$.

Table 7: Reconfiguration accuracy comparison for Test 2

| ROE | Desired ROE, m | Achieved ROE, $J_2 = 0$ | Relative error | Achieved ROE, $J_2$ | Relative error |
|---|---|---|---|---|---|
| $\delta a$ | 0 | 0 | 0% | 0 | 0% |
| $\delta\lambda$ | -10500 | -10498.90 | 0.01% | -10496.74 | 0.03% |
| $\delta e_x$ | 150 | 150.14 | 0.10% | 149.74 | 0.17% |
| $\delta e_y$ | -50 | 3.46 | 107% | -50.47 | 0.95% |

Table 7 shows how the new semi-analytical solution removes large reconfiguration errors in the relative eccentricity vector due to $J_2$ effects on the reference argument of perigee which affect the mean argument of latitude of the maneuvers.

Similar to Test 1, Fig. 7 shows the evolution of the ROE in phase space. The semi-analytical solution meets the delta-v lower bound of 0.117 $\frac{m}{s}$, calculated using Eq. 22, and is thus optimal. Table 8 compares the delta-v obtained by the semi-analytical solution and by the primer vector optimal control algorithm. As a matter of fact, the proposed semi-analytical solution is optimal and represents the minimum path in relative eccentricity vector space.

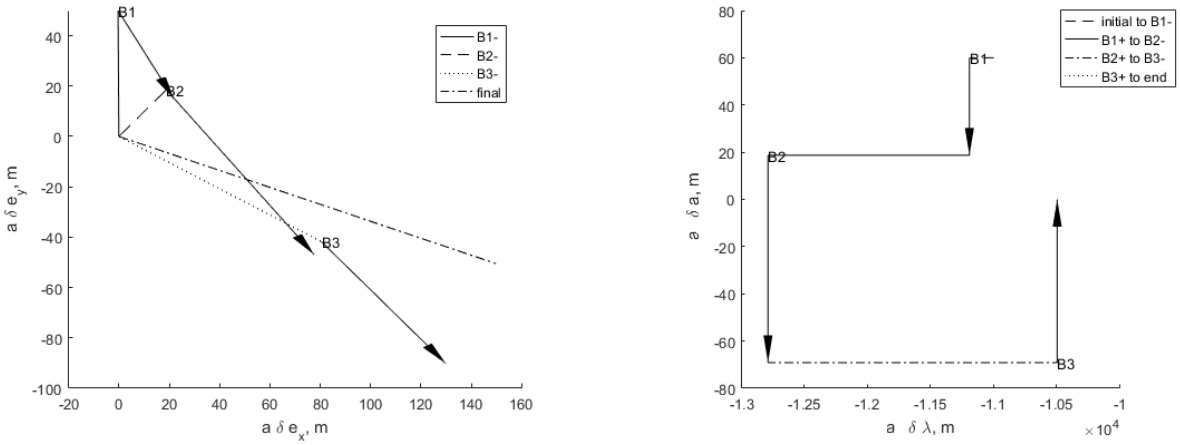


(a) Relative eccentricity vector as affected by maneuvers (arrows) and natural perturbations.

(b) Relative semi-major axis and relative mean longitude as affected by maneuvers (arrows) and natural perturbations.

Figure 7: Evolution of ROE in Test 2 in the presence of $J_2$ effects

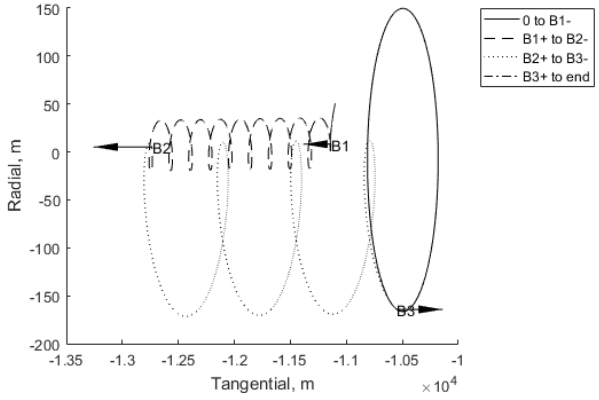


Figure 8: Evolution of relative position in RTN frame

Table 8: Comparison of maneuver schemes calculated using primer vector and semi-analytical solutions

| $k_i$ (Maneuver locations) | Primer vector theory | Semi-analytical solution |
|---|---|---|
| 0 | $-0.0244\frac{m}{s}$ | $-0.0244\frac{m}{s}$ |
| 18 | $-0.0520\frac{m}{s}$ | $-0.0520\frac{m}{s}$ |
| 25 | $0.0410\frac{m}{s}$ | $0.0409\frac{m}{s}$ |
| Total delta-v | $0.1174\ \frac{m}{s}$ | $0.1173\ \frac{m}{s}$ |

### *3. Test 3: Loss of optimality of semi-analytical solutions*

Test 3 is intended to show that the semi-analytical solution becomes suboptimal when $|\Delta\delta\bar{a}| > ||\Delta\delta\bar{\boldsymbol{e}}||$. To this end, the desired change in relative semi-major axis is incrementally increased for a given set of reconfiguration parameters until $|\Delta\delta\bar{a}|$ equals, and then exceeds, $||\Delta\delta\bar{\boldsymbol{e}}||$. The initial chief orbit and reconfiguration parameters are given by

$$
\begin{aligned}
\boldsymbol{\alpha}_{c,0} &= \begin{bmatrix} 6578 \text{ km} & 0 & 8^o & 0 & 30^o & 0 \end{bmatrix} \\
a\delta\boldsymbol{\alpha}_0 &= \begin{bmatrix} 30 & -11000 & 0 & -50 & 0 & 0 \end{bmatrix} \text{ m} \\
a\delta\boldsymbol{\alpha}_f &= \begin{bmatrix} 0 & -10500 & 45 & 70 & 0 & 0 \end{bmatrix} \text{ m} \\
\Delta u &= 5 \text{ orbits}
\end{aligned}
\tag{56}
$$

yielding the following desired change of ROE before and after pre-compensation

$$
\begin{aligned}
\begin{bmatrix} a\Delta\delta a & a\Delta\delta\lambda & a\Delta\delta e_x & a\Delta\delta e_y \end{bmatrix} &= \begin{bmatrix} -30 & 500 & 45 & 120 \end{bmatrix} \text{ m} \\
\begin{bmatrix} a\Delta\delta\bar{a} & a\Delta\delta\bar{\lambda} & a\Delta\delta\bar{e_x} & a\Delta\delta\bar{e_y} \end{bmatrix} &= \begin{bmatrix} -30 & 1884 & 40.4 & 119.8 \end{bmatrix} \text{ m}
\end{aligned}
\tag{57}
$$

Holding all other final ROE constant, $a\Delta\delta\bar{a}$ is then decreased from 0 to -300 m. When $a\Delta\delta\bar{a} = -128.16$ m, $|\Delta\delta\bar{a}| = ||\Delta\delta\bar{\boldsymbol{e}}||$. The total delta-v calculated using Tables 3-4 is compared to the total delta-v calculated via optimal primer vector theory. For all reconfigurations, the maneuvers occur at $k_1 = 0$, $k_2 = 1$, $k_3 = 6$, and the primer vector algorithm is initialized with tentative maneuvers occurring close to the chosen $k_i$ used in the semi-analytical solution. The results are shown in Fig. 9. As expected, the required delta-v is constant up to $|\Delta\delta\bar{a}| = ||\Delta\delta\bar{\boldsymbol{e}}||$, because it is proportional to the desired change of relative eccentricity vector. The limit case where $a\Delta\delta\bar{a} = -128.16$ m is circled in Fig. 9. As $|\Delta\delta\bar{a}|$ becomes greater than $||\Delta\delta\bar{\boldsymbol{e}}||$, the semi-analytical solution produces a suboptimal maneuver scheme. This is evident from the increasing difference between delta-v required by the reference and semi-analytical solutions.

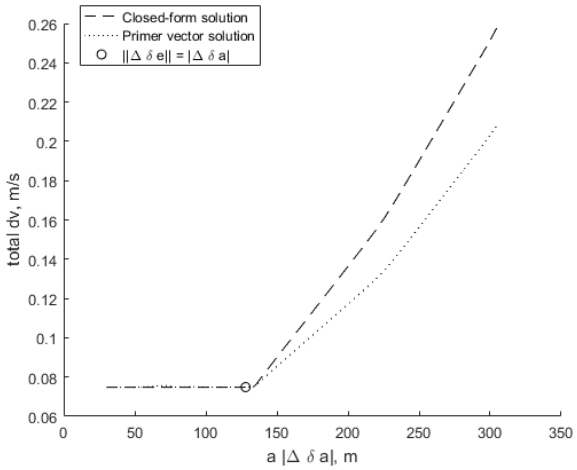


Figure 9: Loss of optimality of in-plane semi-analytical solution for $|\Delta\delta\bar{a}| > ||\Delta\delta\bar{\boldsymbol{e}}||$

## B. Out-of-Plane Control in Perturbed Near-Circular Orbits

### *1. Test 4: High drift of relative inclination vector*

Test 4 shows the benefits of the new out-of-plane semi-analytical control solution given by Eqs. 25 and 26 in the presence of large $J_2$ effects. In particular, when the desired change in the x-component of the relative inclination vector is large, the change of drift of the y-component of the relative inclination vector caused by the cross-track maneuver needs to be taken into account. Consider the natural dynamics of the y-component of the relative inclination vector given by

$$
\delta i_{y,t+\tau} = 2\kappa T\tau\delta i_{x,t} + \delta i_{y,t} \tag{58}
$$

changing $\delta i_x$ during the reconfiguration is equivalent to changing the achieved $\delta i_y$. This effect is proportional to $\kappa T\tau$, which is maximized for low Earth polar orbits. In order to demonstrate the error caused by neglecting $J_2$ in the computation of the out-of-plane maneuver, the initial chief orbit and reconfiguration parameters are given by

$$
\begin{aligned}
\boldsymbol{\alpha}_{c,0} &= \begin{bmatrix} 6828 \text{ km} & 0 & 78^o & 0 & 0 & 0 \end{bmatrix} \\
a\delta\boldsymbol{i}_0 &= \begin{bmatrix} 10 & 70 \end{bmatrix} \text{ m} \\
a\delta\boldsymbol{i}_f &= \begin{bmatrix} 400 & 120 \end{bmatrix} \text{ m} \\
\Delta u &= 7 \text{ orbits}
\end{aligned}
\tag{59}
$$

yielding the following required change of ROE after pre-compensation

$$
a\Delta\delta\bar{\boldsymbol{\alpha}} = \begin{bmatrix} 0 & 0 & 0 & 0 & 390 & 49.4 \end{bmatrix} \text{ m} \tag{60}
$$

Despite the significant drift of the relative inclination vector and the early maneuver execution, Fig. 10 illustrates how the desired ROE are accurately achieved at the end of the reconfiguration.

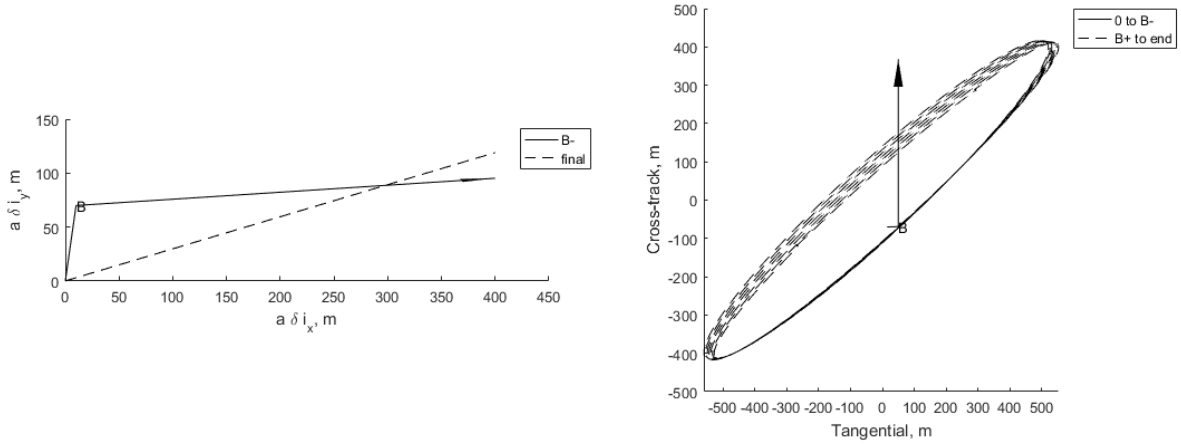


(a) Relative inclination vector as affected by single maneuver and natural perturbations.

(b) Evolution of relative position in along-track/cross-track plane of RTN frame.

Figure 10: Evolution of ROE of Test 4 in the presence of $J_2$ effects

Table 9 shows a comparison between the accuracy of the new semi-analytical solution given by Eqs. 25 and Eq. 26 and previous solutions which do not take into account the effects of $J_2$ besides the pre-compensation.[10] Substantial reduction of the reconfiguration error in the y-component of the relative inclination vector is evident.

Table 9: Reconfiguration accuracy comparison for Test 4

| ROE | Desired ROE, m | Achieved ROE, $J_2 = 0$ | Relative error | ROE achieved, $J_2$ | Relative error |
|---|---|---|---|---|---|
| $\delta i_x$ | 400 | 400.05 | 0.013% | 400.02 | 0.005% |
| $\delta i_y$ | 120 | 144.76 | 20.63% | 119.49 | 0.430% |

The optimality of the result is verified in Table 10 through a comparison of the maneuver size and location provided by the semi-analytical solution and by primer vector theory.

Table 10: Comparison of maneuver schemes calculated using primer vector and semi-analytical solution

| Location (rad), primer vector | Size, primer vector | Location, (rad), semi-analytical | Size, semi-analytical |
|---|---|---|---|
| 0.0670 | $0.4399 \frac{m}{s}$ | 0.0670 | $0.4373 \frac{m}{s}$ |

### C. In-Plane Control in Unperturbed Eccentric Orbits

#### 1. *Test 5: Dominant* $||\Delta\delta\bar{\boldsymbol{e}}||$

To illustrate the optimality of the semi-analytical solution given by Eqs. 38-42, a hypothetical mission to image Beta Pictoris using a miniaturized Distributed Occulter/Telescope (mDOT) is considered.[7] mDOT is deployed in a high elliptical geosynchronous transfer orbit, which has a large apogee radius and low mechanical energy. The initial chief orbit conditions used to simulate this mission are given by

$$\boldsymbol{\alpha}_{c,0} = \begin{bmatrix} 30788 \text{ km} & 0.72 & 39^o & 357^o & 88^o & 0 \end{bmatrix} \tag{61}$$

whereas the in-plane reconfiguration parameters are as follows

$$\begin{aligned} a\delta\boldsymbol{\alpha}_0 &= \begin{bmatrix} 60 & -11000 & 0 & 50 & 0 & 0 \end{bmatrix} \text{ m} \\ a\delta\boldsymbol{\alpha}_f &= \begin{bmatrix} 20 & -10500 & 250 & -50 & 0 & 0 \end{bmatrix} \text{ m} \\ \Delta u &= 7 \text{ orbits} \end{aligned} \tag{62}$$

yielding the following required change of ROE after pre-compensation

$$a\Delta\delta\bar{\boldsymbol{\alpha}} = \begin{bmatrix} -40 & 4435.4 & 250 & -100 & 0 & 0 \end{bmatrix} \text{ m} \tag{63}$$

Tangential maneuvers are executed at $k_i = 0, 1, 6$ to mimic mission operations time constraints. Figure 11 shows the resulting evolution of the in-plane ROE during the reconfiguration span. Note in Fig. 11(a) how the impulsive maneuvers move along the shortest path from $\delta\boldsymbol{e}_0$ to $\delta\boldsymbol{e}_f$. According to the delta-v lower bound from Eq. 21, this is an optimal solution with a total delta-v of $22.6\frac{cm}{s}$.

To further validate optimality, the semi-analytical solution is compared with the optimal solution generated by the primer vector optimal control. Table 11 compares the solutions.

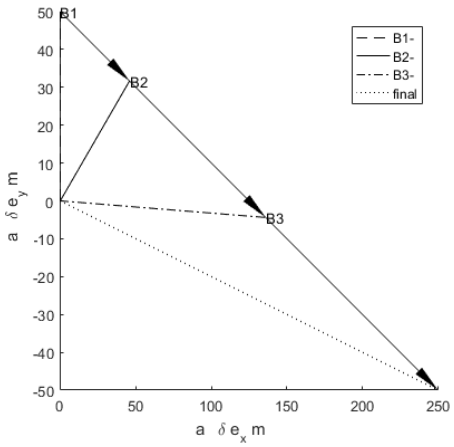


(a) Relative eccentricity vector as affected by impulsive maneuvers and natural dynamics.

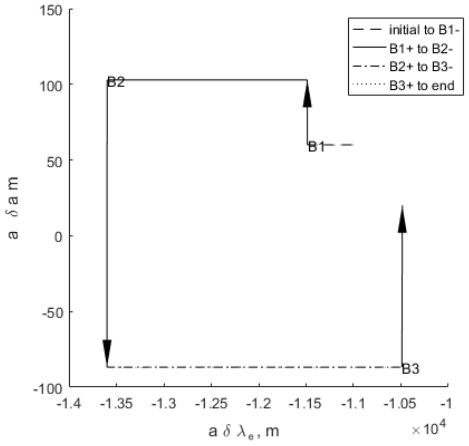


(b) Relative semi-major axis and modified relative mean longitude as affected by impulsive maneuvers and natural dynamics.

Figure 11: Evolution of ROE for Test 5

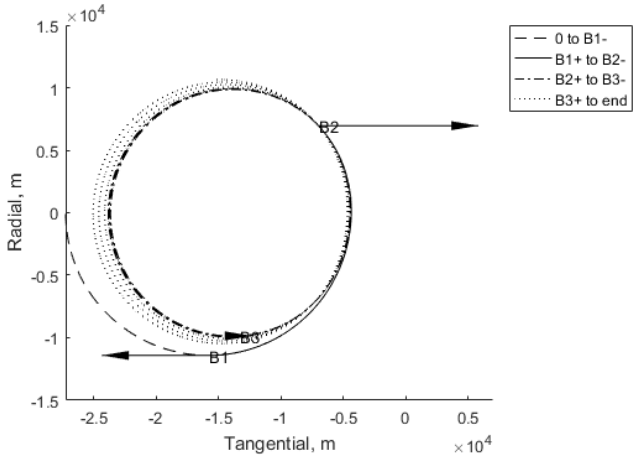


Figure 12: Evolution of relative position in RTN frame

Table 11: Comparison of maneuver schemes calculated using primer vector and semi-analytical solutions

| $k_i$ (Maneuver locations) | Primer vector theory | Semi-analytical solution |
|---|---|---|
| 0 | $-8.68\frac{cm}{s}$ | $-8.62\frac{cm}{s}$ |
| 1 | $11.9\frac{cm}{s}$ | $12.81\frac{cm}{s}$ |
| 6 | $1.18\frac{cm}{s}$ | $0.96\frac{cm}{s}$ |
| Total delta-v | $21.76\frac{cm}{s}$ | $22.4\frac{cm}{s}$ |

*2. Test 6: Loss of optimality of semi-analytical solution*

The semi-analytical solution given by Eqs. 38-42 is optimal for dominant variations of the relative eccentricity vector, given by

$$\frac{\eta^2}{(1+e)}|\Delta\delta\bar{a}| \leq ||\Delta\delta\bar{\boldsymbol{e}}|| \text{ and } \frac{2\eta^2}{3(1+e)\Delta M}|\Delta\delta\bar{\lambda_e}| \leq ||\Delta\delta\bar{\boldsymbol{e}}|| \tag{64}$$

In order to invalidate Eq. 64, Test 6 incrementally increases the desired change in relative semi-major axis of a given set of reconfiguration parameters until $\frac{\eta}{1+e}|\Delta\delta\bar{a}|$ equals, and then exceeds, $\frac{1}{\eta}||\Delta\delta\bar{\boldsymbol{e}}||$. The initial chief orbit and reconfiguration parameters are given by

$$\begin{aligned} \boldsymbol{\alpha}_{c,0} &= \begin{bmatrix} 9000 \text{ km} & 0.25 & 8^o & 0 & 0 & 0 \end{bmatrix} \\ a\delta\boldsymbol{\alpha}_0 &= \begin{bmatrix} 0 & -11000 & 0 & 25 & 0 & 0 \end{bmatrix} \text{ m} \\ a\delta\boldsymbol{\alpha}_f &= \begin{bmatrix} 20 & -10500 & 25 & 50 & 0 & 0 \end{bmatrix} \text{ m} \\ \Delta u &= 5 \text{ orbits} \end{aligned} \tag{65}$$

yielding the total desired change of ROE given by

$$\begin{bmatrix} a\Delta\delta\bar{a} & a\Delta\delta\bar{\lambda}_e & a\Delta\delta\bar{e_x} & a\Delta\delta\bar{e_y} \end{bmatrix} = \begin{bmatrix} 20 & 500 & 25 & 25 \end{bmatrix} \text{ m} \tag{66}$$

Eq. 66 also represents the desired change in ROE after pre-compensation, because the initial relative semi-major axis is zero, and therefore no drift in $\delta\lambda$ is caused over time.

Holding all other desired variations constant, $a\Delta\delta\bar{a}$ is increased. When $a\Delta\delta\bar{a} = 47.1$ m, Eq. 64 is no longer satisfied. $a\Delta\delta\bar{a}$ is then increased past this threshold to show that the semi-analytical solution becomes suboptimal. Fig. 13 illustrates the comparison between the semi-analytical and primer vector solutions in terms of total delta-v. The limit case at which $a\Delta\delta\bar{a} = 47.1$ m is circled.

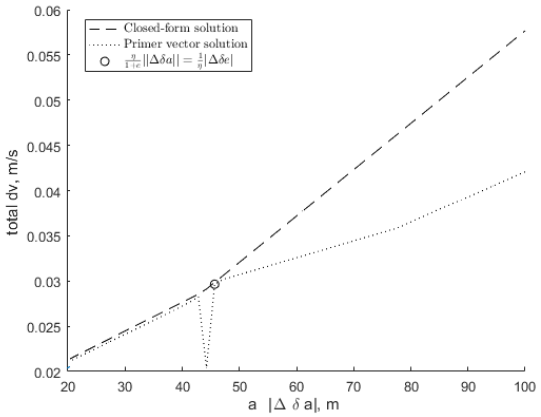


Figure 13: Loss of optimality of in-plane semi-analytical solution for $\frac{\eta^2}{1+e}|\Delta\delta\bar{a}| > ||\Delta\delta\bar{\boldsymbol{e}}||$

The required total delta-v calculated using the semi-analytical solution matches primer vector theory up to the point at which $\frac{\eta}{1+e}|\Delta\delta\bar{a}| = \frac{1}{\eta}||\Delta\delta\bar{\boldsymbol{e}}||$. As $\frac{\eta}{1+e}|\Delta\delta\bar{a}|$ becomes greater than $\frac{1}{\eta}||\Delta\delta\bar{\boldsymbol{e}}||$, the semi-analytical solution produces a suboptimal maneuver scheme, as evident from the plots of Fig. 13. Note the sudden discontinuity in the total delta-v calculated using primer vector theory close to the limit case. This is an example of the poor convergence properties of the primer vector optimal control theory algorithm.

## D. Out-of-Plane Control in Unperturbed Eccentric Orbits

### *1. Test 7: Confirmation of optimality*

Test 7 is intended to confirm that the out-of-plane semi-analytical solution given by Eq. 36 is optimal. The initial chief orbit and reconfiguration parameters are given by

$$\begin{gathered}\boldsymbol{\alpha}_{c,0} = \begin{bmatrix}9000\text{ km} & 0.25 & 78^o & 0 & 0 & 0\end{bmatrix} \\ a\delta\boldsymbol{i}_0 = \begin{bmatrix}30 & 50\end{bmatrix}\text{ m} \\ a\delta\boldsymbol{i}_f = \begin{bmatrix}60 & 10\end{bmatrix}\text{ m} \\ \Delta u = 5\text{ orbits}\end{gathered} \tag{67}$$

yielding the following required change of ROE after pre-compensation

$$a\Delta\delta\bar{\boldsymbol{\alpha}} = \begin{bmatrix}0 & 0 & 0 & 0 & 30 & -40\end{bmatrix}\text{ m} \tag{68}$$

Fig. 14 shows the evolution of the relative inclination vector $\delta\boldsymbol{i}$ in ROE space. The single impulse solution transfers the formation from start to end conditions according to a minimum-length path. The magnitude of the maneuver is $-0.032\frac{m}{s}$, applied at true argument of latitude $\theta = 2.2143$ rad.

Using the benchmark primer vector optimal control algorithm, the magnitude and location of the out-of-plane maneuver are identical to the semi-analytical solution within the expected numerical errors.

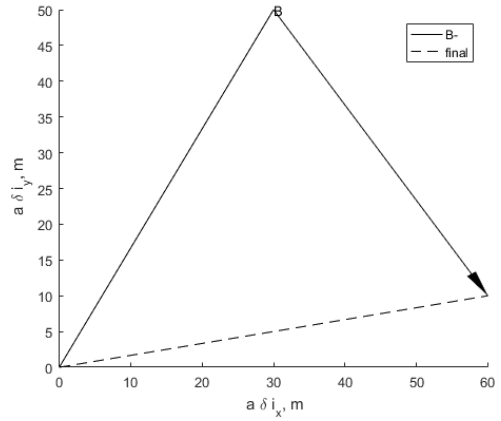


Figure 14: Evolution of ROE for Test 7

# IX. Conclusions

In order to perform increasingly advanced multi-satellite missions in formation-flying, rendezvous, fractionation, and swarming, on-board control must also advance in its ability to arbitrarily reconfigure the relative motion in a fuel-efficient, autonomous, and flexible manner. This paper addressed the computation of fuel-optimal control solutions for formation reconfiguration using impulsive maneuvers. After a formalization of the mathematical framework for optimal guidance and control, new semi-analytical solutions were developed for in-plane and out-of-plane control in near-circular perturbed and eccentric unperturbed orbits. The new semi-analytical solutions for near-circular perturbed orbits allow us to achieve desired reconfigurations with improved accuracy. The new semi-analytical solutions for eccentric unperturbed orbits expand the range of reconfigurations for which we can find fuel-optimal impulsive maneuver schemes, bringing us closer to a generalized solution, applicable to all desired reconfigurations.

A general definition for the delta-v lower bound was derived and used to provide confirmation of the optimality of the new semi-analytical solutions. For further validation of performance and functionality, the new semi-analytical solutions were rigorously validated by numerical integration of the equations of motion and by comparison with primer vector theory optimal control solutions. The results show that the new semi-analytical solutions are always optimal for reconfigurations where the change in relative eccentricity vector is dominant. However, it was also confirmed that the semi-analytical solutions become suboptimal when the change in relative semi-major axis is dominant in most of the cases. A strong analogy between relative and absolute orbit control has been established which suggests that semi-analytical solutions for unperturbed eccentric orbits should be optimal for reconfigurations where initial and final relative eccentricity vector as well as the absolute eccentricity vector are all collinear. Although the Hohmann transfer analogy provided insight into the form of optimal solutions for large changes in relative semi-major axis, the derivation of a new, more robust semi-analytical solution to be applicable to all cases is warranted. Future work includes extension of the semi-analytical guidance and control solutions to perturbed orbits of arbitrary eccentricity.

# Appendix

## A. Primer vector iterative scheme, details

In order to measure the performance of the (semi-)analytical solutions, the primer vector control algorithm is applied as follows. The discrete optimal control problem is initially solved for a large number of impulses. The maxima are determined, as shown in Fig. 15(a), and used to generate an initial primer vector history, shown in Fig. 15(b), according to the method described by Roscoe et al.[19] In order for a solution to be considered optimal, its primer vector history must satisfy the following conditions:[21] 1) The primer vector and its first derivatives are continuous everywhere, 2) The magnitude of the primer vector satisfies $p(t) \leq 1$ with the impulses occurring at those instants at which $p = 1$, and 3) at the impulse times, the primer vector is a unit vector in the optimal thrust direction.

The initial primer vector solution in Fig. 15(b) does not meet the conditions given above and therefore must be improved. Improvements are made iteratively by resolving the discrete-time optimal control problem according to the following modifications:[19] 1) if $\dot{p}(t) \neq 0$ at the time of any impulse, move the impulse slightly in the direction of increasing $p$ ($\dot{p} > 0$), 2) if $p(t) > 1$ somewhere other than in the vicinity of an impulse, add another impulse at the time of maximum $p(t)$, and 3) if $p(t) < 1$ and $\dot{p}(t) = 0$ at the time of any impulse, remove that impulse. Iterations toward optimality are shown in Fig. 15(c). Once the optimality conditions are met, the solution terminates, yielding a final primer vector history with optimal impulsive maneuver times as given in Fig. 15(d). The magnitudes of the maneuvers are found by solving the discrete-time control problem a last time with the optimal maneuver times.

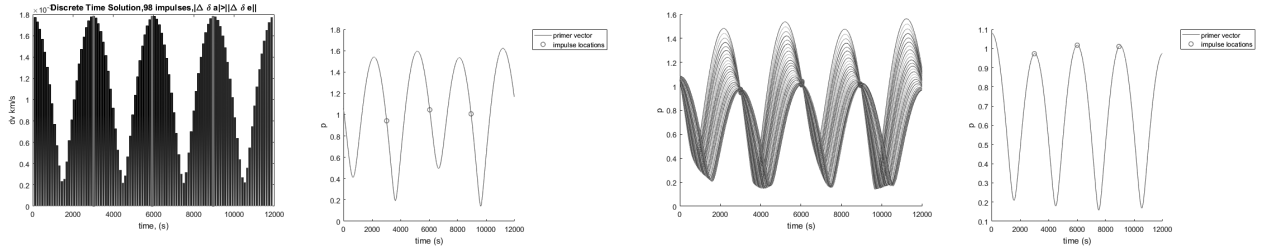


(a) Generation of initial discrete optimal solution with many impulses

(b) Initial primer vector history

(c) Iteration of primer vector solution by resolving discrete optimal control

(d) Final primer vector solution

Figure 15: Primer vector iterative scheme

## References


[1]D'Amico, S., Pavone, M., Saraf, S., Alhussien, A., Al-Saud, T., Buchman, S., Byer, R., Farhat C.,"Miniaturized Autonomous Distributed Space System for Future Science and Exploration," *8th International Workshop on Satellite Constellations and Formation Flying, IWSCFF 2015*, 8-10 June, Delft University of Technology (2015).

[2]D'Amico, S., Ardaens, J.-S., Larsson, R.,"Spaceborne Autonomous Formation-Flying Experiment on the PRISMA Mission,"*Journal of Guidance, Control, and Dynamics*, Vol.35, No. 3, 834-850 (2012). DOI 10.2514/1.55638

[3]Ardaens, J.-S., D'Amico S.,"Spaceborne Autonomous Relative Control System for Dual Satellite Formations,"*Journal of Guidance, Control and Dynamics*, Vol. 32, No. 6, 1859-1870 (2009). DOI 10.2514/1.42855

[4]Ardaens, J.-S., D'Amico, S., Fischer, D.,"Early Flight Results from the TanDEM-X Autonomous Formation Flying System," *4th International Conference on Spacecraft Formation Flying Missions and Technologies*, 18-20 May 2011, St-Hubert, Quebec (2011).

[5]D'Amico, S., Ardaens, J.-S., Gaias, G., Benninghoff, H., Schlepp, B., Joergensen, J. L., "Noncooperative Rendezvous using Angles-only Optical Navigation: System Design and Flight Results,"*Journal of Guidance, Control, and Dynamics*, Vol. 36, No. 6, 1576-1595 (2013). DOI 10.2514/1.59236

[6]Gaias, G., Ardaens, J.-S., D'Amico, S.,"The Autonomous Vision Approach Navigation and Target Identification (AVANTI) Experiment: Objectives and Design,"*9th International ESA Conference on Guidance, Navigation and Control Systems, ESA GNC 2014*, 2-6 June 2014, Oporto, Portugal (2014).

[7]Koenig, A.W., D'Amico, S., Macintosh, B., Titus, C.J.,"Optimal Formation Design of a Miniaturized Distributed Occulter/Telescope in Earth Orbit," *2015 AAS/AIAA Astrodynamics Specialist Conference*, 9-13 August 2015, Vail, Colorado, United States (2015).

[8]Kolmas, J., Banazadeh, P., Koenig, A.W., D'Amico, S., Macintosh, B.,"System Design of a Miniaturized Distributed Occulter/Telescope for Direct Imaging of Star Vicinity," *IEEE Aerospace Conference*, March 5-12, 2016, Yellowstone Conference Center, Big Sky, Montana, United States (2016).

[9]D'Amico, S., "Autonomous Formation Flying in Low Earth Orbit," Ph.D. Thesis, Technical Univ. of Delft, Delft, The Netherlands, March 2010.

[10]Gaias, G., D'Amico, S., "Impulsive Maneuvers for Formation Reconfiguration Using Relative Orbital Elements," *Journal of Guidance, Control, and Dynamics*, Vol. 38, No. 6, pp. 1036-1049 (2015). DOI: 10.2514/1.G000189

[11]Gaias, G., D'Amico, S., Ardaens, J.-S.,"Generalized Multi-Impulsive Maneuvers for Optimum Spacecraft Rendezvous in Near-Circular Orbit," *International Journal of Space Science and Engineering*, Vol. 3, No. 1, 68-88 (2015). DOI: 10.1504/IJSPACESE.2015.069361

[12]Gaias, G., Ardaens, J.-S., Montenbruck, O.,"Model of J2 Perturbed Satellite Relative Motion with Time-Varying Differential Drag," *Celestial Mechanics and Dynamical Astronomy*, Vol. 123, No. 4, 411–433, 2015.

[13]Koenig, A.W., Guffanti, T., D'Amico, S.,"New State Transition Matrices for Relative Motion of Spacecraft Formations in Perturbed Orbits," *AIAA Space and Astronautics Form and Exposition, SPACE 2016*, 13-16 September, 2016, Long Beach Convention Center, California, United States (2016).

[14]D'Amico, S., "Relative Orbital Elements as Integration Constants of Hill's Equations," German Aerospace Center (DLR), Technical Note, 05-08, 2008.

[15]Schaub, H., Junkins, J. L.,"Analytical Mechanics of Space Systems," AIAA, 2003.

[16]Ichikawa, A., Ichimura, Y.,"Optimal Impulsive Relative Orbit Transfer Along a Circular Orbit," *Journal of Guidance, Control, and Dynamics*, Vol. 31, No. 4, 1014-1027 (2008).

[17]Tillerson, M., and How, J.,"Advanced Guidance Algorithms for Spacecraft Formation-Keeping," *Proceedings of the 2002 American Control Conference (IEEE Cat. No.CH37301)*, Vol. 4, pp. 2830–2835 (2002). DOI 10.1109/ACC.2002.1025218

[18]Tillerson, M., Inalhan, G., How, J., "Co-Ordination and Control of Distributed Spacecraft Systems Using Convex Optimization Techniques," *International Journal of Robust Nonlinear Control*, Vol. 12, No. 2-3, 207-242 (2002). DOI 10.1002/rnc.683

[19]Roscoe, C. W. T., Westphal, J. J., Griesbach, J. D., Schaub, H.,"Formation Establishment and Reconfiguration using Differential Elements in J2-Perturbed Orbits," *IEEE Aerospace Conference Proceedings, IEEE Computer Society*, 1-8 March 2014, Big Sky, MT, United States (2014). DOI 10.1109/AERO.2014.6836272

[20]Lawden, D. F., "Optimal Trajectories for Space Navigation," 1963.

[21]Prussing, J.E., "Primer Vector Theory and Applications, In: Conway, B.A. (ed.) Spacecraft Trajectory Optimization," Cambridge University Press, Cambridge (2011).

[22]Gim, D.-W., Alfriend,K. T.,"State Transition Matrix of Relative Motion for the Perturbed Noncircular Reference Orbit," *Journal of Guidance, Control, and Dynamics*, Vol. 26, No. 6, 956–971, 2003.

[23]Anderson, P. V., Schaub, H.,"N-Impulse Formation Flying Feedback Control Using Nonsingular Element Description," *Journal of Guidance, Control, and Dynamics*, Vol. 37, No. 2, 540-548 (2014).

[24]Rogers, A., Woosley, McGwier, R., "Nonlinear Tracking of Optimal Maneuvers in Spacecraft Formations," 1-3 July 2015, American Control Conference, IEEE (2015). DOI 10.1109/ACC.2015.7172258

[25]Vaddi, S.S., Alfriend, K.T., Vadali, S.R. & Sengupta P., "Formation Establishment and Reconfiguration Using Impulsive Control", *Journal of Guidance, Control, and Dynamics*, Vol. 28, No. 2, pp. 262-268 (2005).

[26]Clohessy, W., Wiltshire, R., "Terminal Guidance System for Satellite Rendezvous," *Journal of Aerospace Sciences*, Vol. 27, No. 9, 653–658 (1960).

[27]Jifuku, R., Ichikawa, A., and Bando, M., "Optimal Pulse Strategies for Relative Orbit Transfer Along a Circular Orbit," *Journal of Guidance, Control, and Dynamics*, Vol. 34, No. 5, 1329–1341 (2011).DOI 10.2514/1.51230

[28]Khalil, M., Larbi, B., Stoll, E., "Spacecraft Formation Control using Analytical Integration of Gauss' Variational Equations," *6th International Conference on Astrodynamics Tools and Techniques - ICATT*, March 2016, Darmstadt, Germany (2016).

[29]D'Amico, S., Montenbruck, O., Arbinger, C., Fiedler, H.,"Formation Flying Concept for Close Remote Sensing Satellites," *15th AAS/AIAA Space Flight Mechanics Conference*, AAS 05-156, January 23-27, 2005, Copper Mountain, Colorado (2005).

[30]Riggi, L., D'Amico, S., "Optimal Impulsive Closed-Form Control for Spacecraft Formation Flying and Rendezvous," *2016 American Control Conference*, July 6–8, 2016, Boston, MA, USA (2016).

[31]Sullivan, J., Grimberg, S., D'Amico, S.,"A Survey of Spacecraft Relative Motion Dynamics Models," *Journal of Guidance, Control, and Dynamics*, Submitted, 2016.

[32]Alfriend, T. K., Vadali, S., Gurfil P., How, J., Breger, L.,"Spacecraft Formation Flying: Dynamics, Control, and Navigation," Elsevier Astrodynamics Series, 2010.

[33]Setty, S., Cefola, P., Montenbruck, O., Fiedler, H.,"Investigating the Suitability of Analytical and Semi-analytical Satellite theories for Space Object Catalogue Maintenance in Geosynchronous Regime,". *AAS/AIAA Astrodynamics Specialist conference*, August 11-15, 2013, Hilton Head, South Carolina, United States (2013).

[34]D'Amico, S., Montenbruck, O.,"Proximity Operations of Formation Flying Spacecraft using an Eccentricity/Inclination Vector Separation," *Journal of Guidance, Control and Dynamics*, Vol. 29, No. 3, 554-563 (2006).

[35]Tschauner, J., Hempel, P.,"Optimale Beschleunigungsprogramme fuer das Rendezvous-Manoever," Astronautica Acta, Vol. 10, 296–307 (1964).

[36]Montenbruck, O., Kirschner, M., D'Amico, S., Bettadpur, S.,"E/I-Vector Separation for Safe Switching of the GRACE Formation," *Aerospace Science and Technology*, Vol. 10, No. 7, 628-635 (2006). DOI 10.1016/j.ast.2006.04.001

[37]Guffanti, T.,"A Semianalytical Study on the Satellite Relative Perturbed Motion Modeling in Relative Orbital Elements," Master Thesis, Politecnico Di Milano, 2016.

[38]Lawden, D. F., "Optimal Transfers between coplanar elliptical orbits", *Journal of Guidance, Control, and Dynamics*, Vol. 15, No. 3, 788-791 (1992). DOI http://dx.doi.org/10.2514/3.20909